QATAR UNIVERSITY

COLLEGE OF ENGINEERING

MEASURING GEOMETRICAL TORTUOSITY OF POROUS MEDIA FROM 3D COMPUTED TOMOGRAPHY IMAGES

BY

IMAN TAWFIQ MADHOUN

A Thesis Submitted to the Faculty of

College of Engineering

in Partial Fulfillment

of the Requirements

for the Degree of

Master of Science

January 2017

COMMITTEE PAGE

The members of the Committee approve the Thesis of Iman Tawfiq Madhoun defended on 17/11/2016.

Riyadh Al-Raoush
Thesis/Dissertation Supervisor

Farid Benyhia
Committee Member

Hisham Eid
Committee Member

Khalid Alshibli
Committee Member

Approved:

Khalifa Al-Khalifa, Dean, College of Engineering

ABSTRACT

Tortuosity is an important parameter that has a significant impact on many environmental processes and applications. Flow in porous media, diffusion of gases in complex pore structures, and transmembrane flux in water desalination are examples of the application of the micro-scale parameter. The main objectives of this thesis are to develop functional relationships that relate tortuosity to geometrical and topological parameters of porous media using three-dimensional (3D) computed tomography images, and select the best model that has the best capability to predict geometrical tortuosity. The objectives were achieved by implementing Random Paths MATLAB code that was developed in this work and compared with available Tort3D MATLAB code using high resolution 3D synchrotron computed tomography images of representative porous media. Tortuosity factors were computed from random tortuous paths of connected voxels (Random Paths Code) and tortuous paths derived from 3D medial surface of void space (Tort3D Code). Tortuosity factors were related to geometrical and topological parameters including porosity (∅), median grain diameter (d_{50}), uniformity coefficient (C_u), coefficient of gradation (C_c), sphericity index (S_i), roundness index (R_i), and specific surface area (*SSA*). Tort3D code was validated by comparing measured with predicted tortuosity factors from models reported in the literature. The two codes measured geometrical tortuosity of different sand systems effectively. However, they provided different tortuosity values, since they were developed using different concepts. Models were developed and predicted tortuosity values were compared with measured tortuosity values. Good agreement was

found between predicted and measured tortuosity values with low error (less than 20%). Model 3 that considers ∅, d_{50}, C_u, and C_c has best capability to predict tortuosity compared with other developed models.

TABLE OF CONTENTS

List of Tables

List of Figures

Acknowledgements

I would like to thank my supervisor Dr.Riyadh Al-Raoush for the useful feedback, comments, and remarks through the learning process of this master thesis.

Furthermore, I would like to express my very profound gratitude to Prof. Abdelmagid Hamouda and Dr.Arselene Ayari for the great support, continuous encouragement, and motivation throughout my years of master study. Without their help and support, I would not be able to overcome the difficulties I faced during the study and reach this stage.

Also, I would also like to thank Dr.Ali Ayari for the support and encouragement to finish graduate education.

Finally, I owe more than thanks to my family members for their support and encouragement throughout my life. Without their support and help, it is impossible for me to finish graduate education.

CHAPTER 1. INTRODUCTION

1.1. Overview of Tortuosity

Soil structure elements are quantified by geometrical parameters, such as porosity, roundness, and sphericity (Naveed et al., 2013). One of the geometrical parameters is tortuosity,τ, which is the ratio of the real path distance to the straightest path distance that molecules move from one point to its destination through the internal structure of porous media (Adler, 1992). It provides better understanding of the mechanisms of fluid flow and indications about the structural complexity in porous media. In the literature, tortuosity has been categorized as geometric tortuosity (Yongjin and Boming, 2007; Yu and Li, 2004), hydraulic tortuosity (Ahmadi et al., 2011; Mauret and Renaud, 1997), or electrical tortuosity (Coleman and Vassilicos, 2008; Comiti and Renaud, 1989).

The geometric tortuosity,τ_g, is the ratio of the average length of true paths through the porous media, $< L_g >$, to the straight-line length, L_s, across the porous media in the direction of flow:

$$\tau_g = \frac{< L_g >}{L_s} \qquad \text{(eq. 1.1)}$$

The value of tortuosity is always greater than one. Tortuosity can also be defined as the ratio of the shortest pathway, L_{min}, to the straight-line length, L_s (Adler, 1992). The coefficient of geometric tortuosity, T_g, is the inverse of geometric tortuosity, $T_g = \frac{1}{\tau_g}$, which is less than one (Ghanbarian et al., 2013).

The hydraulic tortuosity, τ_h, can be estimated as the square of the ratio of the flux-weighted average path length for hydraulic flow, $< L_h >$, to the straight-line length, L_s (Clennell, 1997; Ghanbarian et al., 2013):

$$\tau_h = \left(\frac{< L_h >}{L_s}\right)^2 \qquad \text{(eq. 1.2)}$$

Flux-weighted average is one of the methods to calculate the average length of the flow paths. It is the average of the lengths of flow lines for all fluid particles that pass through a cross-section during a specified period. The coefficient of hydraulic tortuosity, T_h, is the inverse of hydraulic tortuosity, $T_h = \frac{1}{\tau_h}$ .The reported value of T_h varies between 0.56 and 0.8 in the literature (Bear, 1972).

The electrical tortuosity, τ_e, is the square of the ratio of the average path length for electrical flow,$< L_e >$, to the straight-line length, L_s, through the pore space (Childs, 1969):

$$\tau_e = \left(\frac{< L_e >}{L_s}\right)^2 \qquad \text{(eq. 1.3)}$$

Electrical resistivity of a medium can be measured to infer the electrical tortuosity as the product of its porosity, $\emptyset$, and the formation factor, F (Coleman and Vassilicos, 2008) as follows:

$$\tau_e = \emptyset F \qquad \text{(eq. 1.4)}$$

F is the quotient of the electrical resistivity of the saturated porous medium, ρ_p, and the resistivity of the saturating liquid, ρ_l. The formation factor is a dimensionless quantity the value of which is always higher than 1 in the absence of solid and/or surface conduction (Ghanbarian et al., 2013).

1.2. Importance of Tortuosity

Transport in unconsolidated porous media is a very important issue that has been investigated by researchers (Civan, 2010; Guo et al., 2015; Manickam et al., 2014; Masciopinto and Palmiotta, 2013; Yuan et al., 2016). It should take into consideration two effects: the decrease of the volume available to fluid transport because of the presence of the solid medium and an increase of the tortuous path that the fluid must flow across it. These effects can be described using the porosity, $\emptyset$, and the tortuosity, τ, parameters (Pisani, 2011). Tortuosity has a significant influence on many applications including simulation models of fluid flow in tight rocks, such as shale gas reservoirs, simulation of regional groundwater flow in a fractured and karstified aquifer, and pollutant transport in fractured aquifers (Masciopinto and Palmiotta, 2013; Yuan et al., 2016).

Some macroscopic transport coefficients (i.e. diffusion coefficient, permeability) are related to important geometrical and topological parameters. For instance, diffusion coefficient is related to tortuosity obtained from diffusion measurements and simulation, τ_d, by the following equation (Grathwohl, 1998):

$$D_p = \frac{\emptyset \ D_b}{\tau_d^2} \qquad \text{(eq. 1.5)}$$

where D_p is the diffusion coefficient in the porous media [L^2 T^{-1}], and D_b is the diffusion coefficient in air or water. Hydraulic tortuosity, τ_h, can be related to permeability, k, using Kozeny-Carman equation (Vervoort and Cattle, 2003) as follows:

$$k = \frac{\emptyset^3}{\beta \ \tau_h^2 \, S^2} \qquad \text{(eq. 1.6)}$$

where $\emptyset$ is the porosity, β is a shape related factor, and *S* is the average pore perimeter. The hydraulic radius is defined by the porosity ($\emptyset$) and the average pore perimeter, *S*. Hydraulic tortuosity (τ_h) and a shape related factor (β) are representative parameters for the actual pore space geometry (Vervoort and Cattle, 2003).

The impact of tortuosity on fluid entrapment has been investigated in the literature (Salmas and Androutsopoulos, 2001). The amount of isolated trapped fluid is important for many applications, including oil reservoir analysis where trapped oil or gas means less production of hydrocarbon, and carbon sequestration problems where trapping of CO_2 leads to safe underground storage (Joekar-Niasar et al., 2013). Fluid entrapment is strongly dependent on the topological properties (pore connectivity and tortuosity) of porous media. In the literature, several models are proposed to express the tortuosity in terms of the pore entrapment fraction, α_{en}, or in terms of (partial) porosity (Androutsopoulos and Salmas, 2000; Salmas and Androutsopoulos, 2001). Salmas and Androutsopoulos (2001) proposed the following relationship between tortuosity and pore entrapped volume fraction through a corrugated pore structure model (CPSM):

$$\tau = 4.6242 \ln\left(\frac{4.996}{1-\alpha_{en}} - 1\right) - 5.8032 \qquad \text{(eq. 1.7)}$$

1.3. Importance of Geometrical Parameters

Geometrical and topological parameters (τ, $\emptyset$, median grain diameter (d_{50}) uniformity coefficient (C_u) coefficient of gradation (C_c) sphericity index (S_i) roundness index (R_i) and specific surface area, *SSA*) have been used to characterize and quantify the soil pore space geometry. Tortuosity is a geometric parameter that influences the transport of water, solutes, and gases in soil (Moldrup et al., 2001). In the literature, tortuosity has been related to $\emptyset$(Rezaee et al., 2007; Shanti et al., 2014; Sun et al., 2013), d_{50} (Naveed et al., 2013), diffusivity, permeability (Moldrup et al., 2001), diffusion (Takahashi et al., 2009), and gas transport parameters (Naveed et al., 2013). Naveed et al. (2013) measured tortuosity, porosity, median grain diameter, coefficient of uniformity, roundness, and sphericity as structure characterization parameters of porous media. Wong (2016) measured C_u to quantify the particle size distribution of weathered soil in Hong Kong. Su et al., (2014) studied the influence of gradation characteristics on the permeability of multi-particle-size sand soil. Vepraskas and Cassel (1987) evaluated R_i and S_i for 50 soil samples to determine relationships of R_i and S_i to the soils' cone index (mechanical impedance), bulk density, and the dense soil angle of repose. Specific surface area (*SSA*) influences many physical and chemical soil properties, such as cation exchange capacity, clay content, organic matter content, porosity and hydrodynamic and geotechnical characteristics (Feller etal., 1992; Petersen et al., 1996; Theng et al., 1999; Yukselen-Aksoy and Kaya, 2010).

1.4. Thesis Organization

This report has several sections as follow: measurements of tortuosity, types of tortuosity models in the literature, models of different tortuosity types, description of and comparison between Tort3D and Random Paths codes, the steps followed to model tortuosity with geometric parameters, a detailed discussion about the developed tortuosity models, selection of the best model to measure tortuosity for different porous systems, and model validation. The final section provides a comparison between tortuosity values obtained from developed Model 1 with tortuosity values predicted by models in the literature.

1.5. Objectives

The main objectives of this thesis are to develop functional relationships that relates tortuosity to geometrical and topological parameters of porous media, and select the best model that has the best capability to predict geometrical tortuosity. These objectives were achieved as follows:

1. measure geometrical tortuosity (τ) using Tort3D code (existing code) using three-dimensional (3D) computed tomography images
2. develop MATLAB code using different algorithm to measure geometrical tortuosity from three-dimensional (3D) segmented binary images of porous systems and compare it with Tort3D code measurements.

CHAPTER 2. BACKGROUND AND LITERATURE REVIEW

2.1. Tortuosity Measurements

Several analytical, experimental, and numerical approaches have been attempted to measure tortuosity. Various numerical approaches estimated tortuosity successfully. One of these approaches was modeling geometric tortuosity as a function of porosity for fixed bed of randomly packed identical particles that have same size and pores of a range of discrete sizes (Lanfrey et al., 2010; Li and Yu, 2011). Ahmadi et al. (2011) proposed analytical expressions for tortuosity and permeability based on the concept of representative volume elementary (REV) of cubic array of spheres. However, calculating tortuosity analytically requires solving complicated mathematical equations (e.g. Yu and Li, 2004; Feng et al., 2007; Lanfrey et al., 2010; Du Plessis and Masliyah, 1991; Ahmadi et al., 2011; Duda et al. , 2014).

Tortuosity can be determined indirectly by performing experiments on fluid diffusion (Corrochano et al., 2014; Gao et al., 2014; Soukup et al., 2015). One of the purposes of measuring tortuosity experimentally is to evaluate the impact of key transport parameters (porosity, pore diameter, tortuosity) on the migration rates of representative underground coal gasification (UCG) related products and contaminants through porous media (Soukup et al., 2015). Soukup et al. (2015) found that porosity, pore diameter, and tortuosity play a significant role in permeation transport of gaseous contaminants compared with physical properties, such as temperature and pressure. The propagation rates of gaseous contaminants in porous soil are lower as tortuosity increases. Another method of obtaining tortuosity experimentally is by measuring electrical conductivity (Coleman and Vassilicos, 2008; Morin et al., 2010).

Although many studies used experimental approaches to measure tortuosity, this method requires special equipment and it takes long time to measure some complicated parameters, such as conductivity and pore size (Sun et al., 2013).

Tortuosity has been determined numerically to characterize the internal structure of porous media (Naveed et al., 2013) and compute Macro-pore network characteristics (e.g. macro-porosity, connectivity, and tortuosity) (Larsbo et al., 2014). Several studies have been conducted to study the relationships between tortuosity and other parameters, such as porosity (Rezaee et al., 2007; Shanti et al., 2014; Sun et al., 2013), diffusivity, permeability (Moldrup et al., 2001), diffusion (Takahashi et al., 2009), and gas transport parameters (Naveed et al., 2013).

Matyka et al. (2008) determined numerically the relationship between the hydraulic tortuosity and porosity in a two-dimensional porous medium arranged as a collection of uniform, randomly distributed and overlapping squares. The relationships found in this study are limited to porous systems of randomly distributed obstacles of equal shape and size. They determined tortuosity of the flow by generating a porous matrix of a known porosity; solving the flow equations in the low Reynolds number regime; and finding the flow streamlines through computer simulations.

Sun et al. (2013) used numerical tools to determine tortuosity factor of a 2D representative elementary volume (REV) of circular particles. The method used to calculate tortuosity has several assumptions: 2D homogenous porous media, which do not represent real porous media system; using spherical particles of low-permeability porous media; arrangement of particles is periodical; and fully saturated pores by an incompressible fluid containing some kinds of solute. Sun et al. (2013) proposed a general model that relates tortuosity and porosity as follows:

$$\tau = 1 - p \ln \emptyset \qquad \text{(eq. 2.1)}$$

The values of p ranged between 0.357 and 0.503.

X-ray computed tomography imaging is considered as a powerful technique to image a real porous media system. Recently, extensive research has been conducted to measure tortuosity using both 2D and 3D CT imaging (Naveed et al., 2013; Promentilla et al., 2009; Shanti et al., 2014; Takahashi et al., 2009). Wide range of computing algorithms and software have been developed to measure tortuosity and other geometrical parameters of porous media from X-ray images, including Medial axis (Peng et al., 2014; Takahashi et al., 2009), Dijkstra algorithm (Shanti et al., 2014), Random Walk simulation (Hu et al., 2013; Promentilla et al., 2009), P-T average method, Fast marching method, Thin-line skeleton (Pardo-Alonso et al., 2014), and A-star algorithm (Dechter and Pearl, 1985).

Medial axis is a common algorithm implemented to analyze the geometric structure of void space in porous media. The medial axis traces the fundamental geometry of the void pathways (Lindquist et al., 1996). It has been implemented to measure tortuosity by calculating the midline path of the pores from 3D CT images of porous media (Reed et al., 2010; Takahashi et al., 2009). For example, Naveed et al. (2013) used Media Axis algorithm to compute tortuosity for images of several sand systems, and they compared their work with experimental gas transport parameters. Reed et al. (2010) used Medial Axis algorithm to measure sand sediment tortuosity from 43 mm^3 X-ray micro-focus computed tomography (XMCT) images and they found tortuosity values for 15 samples ranged from 1.332 to 1.3337.

Medial axis algorithm has some disadvantages. The algorithm is sensitive to small changes in the boundary of the object. Small changes in the object's boundary can lead to a large change in the skeleton (Cornea et al., 2007). The most common software that performs image processing and skeletonization is 3DMA. Ngom et al. (2011) used 3DMA software using obtained X-ray micro-tomography data to develop geometrical model of the pore space of soil aggregates (10% sand, 70% silt, and 20% clay). 3DMA software determines length, pore radius distribution, and tortuosity as geometrical characteristics. Ngom et al. (2011) compared their obtained results with previous statistics of pore space using the same software. They obtained similar trends towards a difference between the two soil structures. Shanti et al. (2014) studied non-destructive 3D imaging of Al_2O_3 porous media using synchrotron X-ray micro-computed tomography and measured connectivity and tortuosity. They performed tortuosity calculations using two methods: the path length ratio (PLR) and gas phase flux (GPF) methods. Skeletonized method was used to calculate the length of the shortest path between nodes through the pore networks (L) and the end -to- end length of the pore channel (R) using an algorithm described previously (Shanti, 2010). R distance was calculated for pair of nodes selected randomly. L distance was calculated using a Dijkstra algorithm (Dijkstra, 1959). The other method GPF depends on finite difference method to simulate gas phase transport through diffusion. For samples of porosity of 0.308 to 0.496, the connectivity values ranged from 0.945 to 0.996. The tortuosity value was 1.5 for alumina with porosity of 0.496. The processing time for tortuosity measurements using PLR and GPF was found to be influenced by the change in porosity.

Some of the available software measure tortuosity are most computationally expensive. For example, the Dijkstra shortest path algorithm in 3DMA-Rock runs for 30 hours or more to compute throats on a Berea image of size of 450x450x450 voxels (Prodanovic and Lindquist). Also, Dijkastra has other disadvantage that it most often cannot obtain the correct shortest ("Dijkstra's algorithm, Bellman Ford algorithm, Single-source shortest paths; Dijkstra algoritması nedir - Bellman Ford algoritması nedir," 2014). Avizo software has been used for 3D macro-pore network quantifications and to measure tortuosity. Keller et al. (2015) considered clay rocks as a mixture of components consisting of impermeable non-clayey sand grains. They analyzed geometric parameters, which control diffusion at larger scales. They constructed X-ray computed tomography images of clay rock samples and applied diffusion simulations to quantify the mesostructured impacts on diffusion.

Promintella et al. (2009) used Random Walk simulation in 3D images to quantify diffusion tortuosity for cement paste of several ages (2, 7, 28 days). Bo Hu et al. (2013) implemented Random Walk Simulation to calculate macroscopic transport properties, such as permeability, specific surface, and tortuosity for two sandstones, a limestone (homogeneous natural stones), three concretes, and brick (heterogeneous materials). All the measurements were limited to 2D X-ray images.

Chung et al. (2015) investigated the spatial distribution of voids in a concreate and two cement paste specimens using X-ray images. They implemented A-star algorithm to calculate the length of the shortest path between inlet and outlet surfaces (Dechter and Pearl, 1985). The heuristic function H for A-star algorithm must be selected carefully in order to make sure of the shortest and lowest cost path (Al-Arif et al., 2012).

The analytical, experimental, numerical approaches in the literature have been found to be successful approaches to measure tortuosity of porous media systems. However, number of limitations is associated with these studies as follows: (1) numerical approaches determines tortuosity for an ideal system, which does not represent real porous media system; (2) there are many complications associated with the numerical approaches; (3) obtaining experimental measurements takes long time to perform and requires specialized equipment; (4) some software (i.e. Avizo) are not readily available to researchers, because they cost thousands of dollars; and (5) Some algorithms (Dijkstra shortest path algorithms in 3DMA) require to run for long time to compute tortuosity ("Dijkstra's algorithm, Bellman Ford algorithm, Single-source shortest paths; Dijkstra algoritması nedir - Bellman Ford algoritması nedir," 2014).

Although, there are several algorithms and software implemented to measure tortuosity from X-ray computed tomography images; there is still a need to develop an efficient and less time consuming algorithm to identify all possible tortuous paths. This thesis presents a new Tort3D MATLAB code to measure geometric tortuosity from 3D X-ray computed tomography images for irregular shaped materials. The code reads segmented images and implements some image processing steps to identify all possible tortuous paths in porous systems. The thesis demonstrates the applicability of the code for real applications by comparing code tortuosity measurements for natural sand systems with tortuosity values predicted by models reported in the literature.

2.2. Models for Determining the Tortuosity in the Literature

2.2.1. Theoretical Models

Tortuosity can be determined theoretically, experimentally, or analytically. Determining tortuosity through theoretical approches is based on specific model of porous media structure. The theoretical models are develpoed based on assumption of ideal system, which considers major limitation. A gathering of randomly capillaries cutting through a solid body is the simplist case of the theoretical models (Ballal and Zygourakis, 1985; Bhatia, 1985; Dykhuizen and Casey, 1989; Shen and Chen, 2007). Table 2.1 presents some theoretical correlations between tortuosity and porosity with the conditions of the physical system on which each correlation is based. These correlations satisfy the following three requirements (Shen and Chen, 2007):

- $\tau^2 \geq 1$
- $\lim_{\emptyset \to 1} \tau = 1$
- $\tau = \frac{\Delta l}{\Delta x}$

where Δl is the actual distance travelled by the species and Δx is the unit length of the medium.

Table 2.1 Theoretical Relations of Tortuosity and Porosity

Model		Condition	Description	References
$\tau^2 = \frac{(3-\emptyset)}{2}$	(eq. 2.2)	Ordered packings	Theoretical	(Akanni et al., 1987; Maxwell, 1881)
$\tau^2 = \frac{(3-\emptyset)}{2}$	(eq. 2.3)	Random homogenous isotropic sphere packings	Theoretical	(Neale and Nader, 1973)
$\tau^2 = 2 - \emptyset$	(eq. 2.4)	A hyperbola of revolution	Theoretical	(Ballal and Zygourakis, 1985; Rayleigh, 1892)
$\tau^2 = \emptyset^{-\frac{1}{3}}$	(eq. 2.5)	Partly saturated homogenous isotropic monodisperse sphere packings	Theoretical	(Millington, 1959; van Brakel and Heertjes, 1974)
$\tau^2 = 1 - \ln\frac{\emptyset}{2}$	(eq. 2.6)	Overlapping spheres	Theoretical	(Akanni et al., 1987; Ho and Striender, 1981; van Brakel and Heertjes, 1974; Weissberg, 1963)

$\emptyset$ is the porosity

2.2.2. Empirical Models

As discussed earlier, theoretical models do not describe real porous systems. Empirical models offer better description the porous systems. Table 2.2 lists some empirical correlations for different soils, sand, and sediment that contain adjustable parameters. Experimentally, the tortuosity of a sediment can be obtained by measuring the porosity ($\emptyset$) and the formation resistivity factor (F), as noted earlier.

Table 2.2 Emprical Relations between Tortuosity and Porosity

Model		Condition	Description	References
$\tau^2 = (\mathrm{A}\,\emptyset^{1-m})^n$	(eq. 2.7)	Sands, muds	Empirical	(Nriagu, 1979; Ullman and Aller, 1982)
$\tau^2 = \emptyset + \mathrm{B}\,(1-\emptyset)$	(eq. 2.8)	Soils, catalysts	Empirical	(Iversen and Jørgensen, 1993; Low, 1981)
$\tau^2 = 1 - \mathrm{C}\ln\emptyset$	(eq. 2.9)	Fine-grained unlithified sediments	Empirical	(Boudreau, 1996; Weissberg, 1963)

A, *m*, *n*, B, and C are adjustable parameters

2.2.3. Numerical Models

Another important common approach to determine tortuosity is by adopting computed algorithim on X-ray computed tomography images. For instance, Naveed et al. (2013) used Media Axis algorithm to compute tortuosity for images of several sand systems, and they developed tortuosity correlation as a function of median grain diameter, d_{50}, as given in Table 2.3.

Table 2.3 Numerical Relation between Tortuosity and Median Grain Diameter

Model		Condition	Description	References
$\tau = 0.19\,\mathrm{d}_{50} + 1.45$	(eq. 2.10)	Sands	Numerical, Medial Axis Algorithm	(Naveed et al., 2013)

2.3. Models for Different Types of Tortuosity

2.3.1. Geometric Tortuosity

Models of geometric tortuosity have been widely developed based on specific properties, such as geometric and topological properties of a porous medium. These models describe the geometric characteristics of the flow path. The developed models are limited to specific artificial porous media as shown in Table 2.4. For instance, Yu and Li (2004) proposed a tortuosity model as a function of porosity for a porous medium consisting of two-dimensional square solid particles, given by eq. 2.11. The model has been developed based on the assumption that some particles in the system are unrestrictedly overlapped.

Feng et al. (2007) proposed an analytical tortuosity expression as a function of porosity assuming a hierarchical structure in a saturated porous medium (eq. 2.12). Lanfrey et al. (2010) developed a theoretical tortuosity model of a fixed bed of randomly packed identical particles as function of porosity ($\emptyset$) and shape factor (ε). They assumed that tortuous paths are represented by sinuous tubes with constant perimeter and cross-sectional area. A shortcoming of the developed model is that as $\emptyset \rightarrow 1$, $\tau \rightarrow 0$; which unrealistic since tortuosity must be limited to 1, and the tortuosity cannot be <1 by definition. Lanfrey et al. (2010) found that tortuosity increases when shape factor or porosity decreases and does not depend on the packing particle size (eq. 2.15).

Naveed et al. (2013) proposed a numerical model of tortuosity as a function of median particle diameter (d_{50}) for Accusand (rounded) and Granusil (angular) sands. Tortuosity values were determined using Medial Axis algorithm in 3DMA-Rock package and they found that tortuosity ranged from 1.5 to 1.75 (Accusand) and 1.48 to 1.65

(Granusil). The model was derived at air-dried and tightly packed conditions using X-ray CT.

2.3.2. Hydraulic Conductivity Models

Empirical and analytical equations have been developed to describe tortuosity in porous media. Matyka et al. (2008) studied the tortuosity- porosity relation for a porous medium consists of freely overlapping squares (eq.2.18). The relation can be re-written in terms of hydraulic radius and specific surface area (eq.2.19). The applicability of these relations is restricted to system of randomly distributed obstacles of equal shape and size. Mota et al. (2001) developed an empirical tortuosity–porosity ($\tau - \emptyset$) power law for binary mixtures of spherical particles (eq.2.20). They measured the conductivity of porous media and found b = 0.4. The exponent must be determined experimentally or numerically which makes a problem with empirical models. Du Plessis and Masliyah (1991) developed an analytical model for isotropic granular porous media using volume-averaging approach. Note that the saturated hydraulic tortuosity in eq. 2.21 ranges between 1 and 1.5 and does not include critical porosity for macroscopic connectivity, in the system.Ahmadi et al. (2011) also presented an analytical function of tortuosity of regular cubic array of mono-sized spheres using a volume-averaging concepts (eq. 2.22).

Pisani (2011) simulated a diffusion process by using a numerical method and expressed the tortuosity with the porosity and the shape factor, the procedure was simple. When solid objects have a low density, the tortuosity of cubic particles was given in eq.

2.23. However, when the solid objects have a high density, the tortuosity of cubic particles was given in eq. 2.24.

Iversen and Jørgensen (1993) proposed tortuosity-porosity relation for Sandy marine sediment based on difussion measurments for high voidage sandy marine sediments, applicable for porosity 0.4-0.9. Mauret and Renaud (1997) proposed tortuosity correlation (eq.2.26) based on conductivity measurements applicable for high voidage bed of spheres. Mauret and Renaud (1997) indicated that torutosity model coefficent of 0.49 is more applicable than the coeffienct of 0.41 proposed by Comiti and Renaud (1989) for tortuosity model. The equation is appicable for porosity 0.36-1.

2.3.3. Electrical Conductivity Models

Maxwell (1873) developed an equation for the electrical conductivity of a conducting medium having a dilute suspension of nonconducting spheres based on the solution of Laplace's equation for steady-state conduction (eq. 2.27).

The equation implies that as $\emptyset \rightarrow 0, \tau_e \rightarrow 1.5$.

Coleman and Vassilicos (2008) studied inviscid and irrotational flow through frractal porous media in two and three dimensions. They proposed an analytical model for tortuosity as a function of porosity ($\emptyset$), fractal dimension (D_f), random walk dimension (D_w), and Euclidean dimenstion (d_E).

Table 2.4 Tortuosity Models in the Literature

Type of Model	Model	Condition	Description	Reference
Geometric Models	$\tau_g = \frac{1}{2}\left[1 + \frac{1}{2}\sqrt{1-\phi^{*}} + \frac{\sqrt{\left(1-\sqrt{1-\phi}\right)^2 + \frac{(1-\phi)}{4}}}{1-\sqrt{1-\phi}}\right]$ (eq. 2.11)	Porous media contains 2-D square solid particles	Analytical	(Yu and Li, 2004)
	$\tau_g = \int_{r_{min}}^{r_{max}} \tau(r) f(r) dr \approx \frac{D}{D + D_T - 1}\left(\frac{L_s}{r_{min}}\right)^{D_T - 1}$ (eq. 2.12) $\tau(r)^{**} = \left(\frac{L_s}{r}\right)^{D_T - 1}$ (eq. 2.13) $f(r) = D\, r_{min}^{D}\, r^{-1-D}$ (eq. 2.14)	Hierarchical structure in a saturated porous media	Analytical	(Feng et al., 2007)
	$\tau_g = 1.23\, \frac{(1-\phi)^{\frac{4}{3}}}{\xi^{2***}\, \phi}$ (eq. 2.15)	Fixed bed of randomly packed identical particles	Theoretical	(Lanfrey et al., 2010)
	$\tau = 0.19\, d_{50}^{****} + 1.45$ (eq. 2.16)	Equation derived for Granusil and Accusand sand, which scanned at air-dried and tightly packed conditions using X-ray CT	Numerical	(Naveed et al., 2013)
Hydraulic Conductivity Models	$\tau_h = 1 - P^{*****} \ln(\phi)$ (eq. 2.17)	3-D porous media, wood chips, platy particles , and high-porosity beds	Empirical	(Pech, 1984)

*ϕ is the porosity
** where $\tau(r)$ is the tortuosity for a pore pathway , L_s is straight line length , $f(r)$ is the pore size probability density function , D is he fractal dimension of the pore size , r_{min} and r_{max} are the smallest and largest pore radii , D_T is the tortuosity fractal dimension, which is between 1 and Euclidean
*** ξ is the sphericity equal to 1 for sphere and < 1 for non-spherical particles
**** d_{50}: median grain diameter (mm), ***** P is an experimental constant 1.6 for wood chips, 0.86 to 3.2 for plates with different height /side ratios and 0.49 for a capillary model of high-porosity beds of spheres and fibers

Table 2.5 Tortuosity Models in the Literature (cont.)

Type of Model	Model	Condition	Description	Reference
Hydraulic Conductivity Models	$\tau_h - 1 \propto \ln\emptyset$ (eq. 2.18) $\tau_h - 1 \propto \frac{RS*}{\emptyset}$ (eq. 2.19)	2-D porous media, freely overlapping square	Numerical	(Matyka et al., 2008)
	$\tau_h = \phi^{-\beta^{**}}$ (eq. 2.20)	3-D porous media, binary mixtures of spherical particles	Empirical	(Mota et al., 2001)
	$\tau_h = \frac{\phi}{1-(1-\phi)^{\frac{2}{3}}}$ (eq. 2.21)	3-D porous media, isotropic granular media	Analytical	(Du Plessis and Masliyah, 1991)
	$\tau_h = \sqrt{\frac{2\,\phi}{3\,[1-B^{***}\,(1-\phi)^{\frac{2}{3}}]}} + \frac{1}{3}$ (eq. 2.22)	3-D porous media, cubic packing and tetrahedral packing	Analytical	(Ahmadi et al., 2011; Duda et al. , 2014)
	$\tau = [1 - 0.64(1-\emptyset)]^{-1}$ (eq. 2.23)	Solid objects have a low density	Numerical method	(Pisani, 2011)
	$\tau = 1 + 0.64(1-\emptyset)$ (eq. 2.24)	Solid objects have a high density	Numerical method	(Pisani, 2011)
	$\tau = 1 - 0.49\ln\emptyset$ (eq. 2.25)	bed of sphere, applicable for $0.36 < \emptyset < 1$	Experimental measurement	(Mauret and Renaud, 1997)

* R is hydraulic radius of granules; S is specific surface area.
** β is a constant equal to 0.4 resulted from measuring the conductivity of porous media
*** B is a constant equal to 1.209 for cubic pickings and 1.108 for tetrahedral packing

Table 2.6 Tortuosity Models in the Literature (cont.)

Type of Model	Model	Condition	Description	Reference
Hydraulic Conductivity Models	$\tau = \sqrt{1 + 2(1 - \emptyset)}$ (eq. 2.26)	Sandy marine sediment, 0.4< $\emptyset$ <0.9	Experimental (diffusion experiment)	(Iversen and Jørgensen, 1993)
	$\tau_e = 1 + \frac{1}{2}(1 - \phi)$ (eq. 2.27)	3-D porous media contains a dilute suspension of non-conducting spheres	Analytical	(Maxwell, 1873)
Electrical Conductivity Models	$\tau_e = \phi^{(D_w{}^{*} - 2)/(D_f - d_E)}$ (eq. 2.28)	2-D and 3-D fractal media	Analytical	(Coleman and Vassilicos, 2008)

*D_w is the random walk fractal dimension, D_f is the fractal dimension, d_E is the Euclidean dimension

Numerous models of tortuosity have been developed as a function of porosity, shape factor, or median grain diameter. However, no study had been carried on to investigate the relationship between tortuosity and a combination of geometric parameters (porosity, median grain diameter, uniformity coefficient, coefficient of gradation, sphericity index, roundness index, and specific surface area). The main objectives of this thesis are to develop new functional relationships between geometrical tortuosity and geometrical parameters and select the best model that has the best capability to predict geometrical tortuosity.

CHAPTER 3. METHODOLOGY

A number of steps were followed to achieve the objectives of this thesis. Tortuosity was computed using two codes: Tort3D (existing) and Random Paths (developed) codes. The two codes were developed using different concepts. Then, the physical properties of the porous media systems were obtained from Al-Raoush (2014). Then, six tortuosity models were generated to relate tortuosity with other geometrical parameters. The coefficient parameters in the six models were calculated in Matlab using Inlinfit function. A very large number of models were developed for each type of tortuosity models and only the best models were selected and shown in this thesis. The predictions of the six developed models were compared based on the validation criteria described in Chapter 4. Also, they were validated by comparing predicted tortuosity using developed Model 1 and models reported in the literature.

3.1. Description of Tort3D Code

The key functionality of Tort3D code is its capability to compute the geometric tortuosity from 3D images of porous media using MATLAB. The code is a user-friendly and straightforward to use where input parameters and user interaction are minimized. It can be used to compute tortuosity from 2D or 3D images. The code has the option of setting the connectivity and tortuosity computations along a given direction (i.e., x, y, or z). Moreover, it is computationally efficient and it is optimized where loops, nested loops, and "if" conditions are limited.

The general flow chart of the algorithm is shown in Figure 3.1. The algorithm commences by reading binary (i.e. segmented) images. Note that the segmentation process is beyond the scope of this thesis as there are many published papers that present and discuss different segmentation algorithms (Feng et al., 2016; Guéguen, 2001; Haindl and Mikeš, 2016; Ilunga-Mbuyamba et al., 2016; Oliveira et al., 2016; Thorp et al., 2016; Touil and Kalti, 2016). The main idea of the algorithm presented herein is that it conducts a guided search for connected paths in the image utilizing the medial surface of the void space. The advantage of this approach is that it limits the search along the medial surface and thus minimizes time and memory requirements to find possible paths in the image.

Once all connected paths are identified for a specific direction, tortuosity is computed as the average of all connected paths in that direction. A connected path is defined as the one that starts from the first slice of the image and ends at the final slice of the image in the direction computation (i.e. flow). The code computes tortuosity as:

$$\text{Tortuosity} = \frac{\text{Average of all path lengths}}{\text{Size of the image in the direction of flow}} \qquad \text{(eq. 3.1)}$$

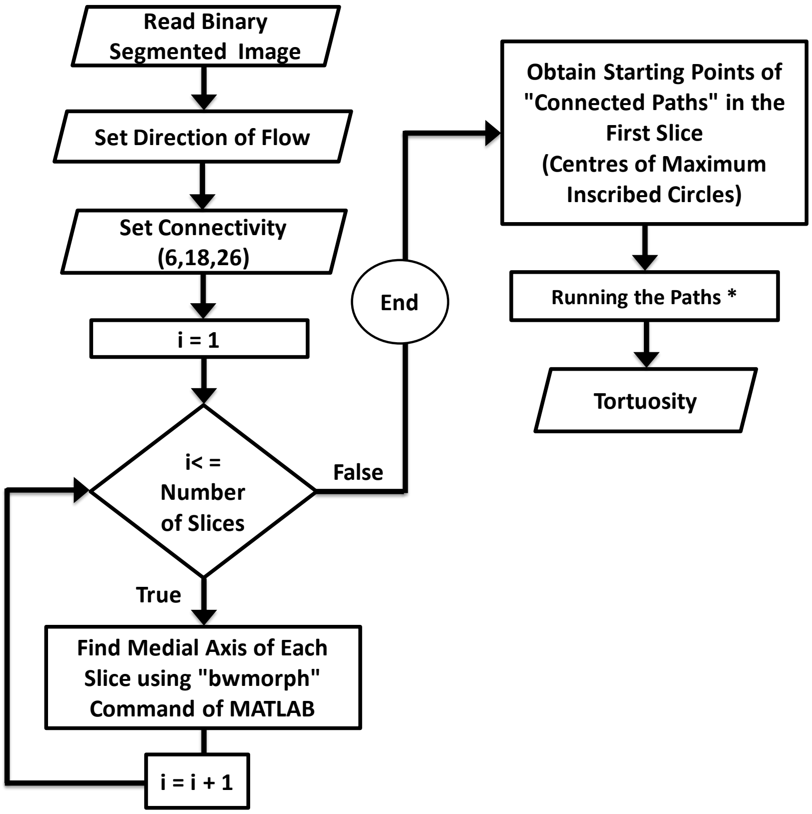

Figure 3.1 Flow Chart of the Main Sections in the Algorithm Developed to Compute Tortuosity from 3D Images

* Running the Paths Section Explained in Details in Figure 3.2

The input and output variables are listed in Table 3.1. The initial step is introducing the input variables to the code as follows: reading binary segmented image, and specifying flow direction (1 for 1D, 2 for 2D, 3 for 3D) and connectivity. The code determines the location of starting points, number of possible paths, image of 3D paths, and measured tortuosity.

Table 3.1 List of Tort3D Code Input and output Variables

Input Variables	
"Raw_image"	Binary segmented image
"Direction_flow"	Direction of flow (1 for flow in the x direction ,2 for the flow in y direction ,3 for the flow in z direction)
"Connect"	Connectivity type (4,8 in 2D or 6,18,26 in 3D)
Output Variables	
"Path_ID"	Number of possible path
"Starting_Paths"	Location of starting points
"3D_ paths"	Image of all tortuous paths
"Tortuosity"	Average geometric tortuosity

3.1.1. Connectivity of Voxels

Identifying connected paths along the medial surface of 3D images depends on the connectivity of voxels. The algorithm defines connectivity of a given voxel (or pixel (image element for 2D) by identifying its neighboring voxels (image volume for 3D) that connects through a face, edge or corner. In 2D images, there are 4 or 8 neighboring pixels for a given pixel, whereas there are 6-connected, 18-connected, and 26-connected for 3D connectivity. The developed code runs at connectivity of 26. However, the connectivity can be changed before searching for tortuous paths.

3.1.2. Skeletonization

Three-dimensional medial surface of the void space is created by 2D skeltonization of the void space of each slice in the image. The MATLAB command "bwmorph" was used to perform the 2D skeltonization for each slice. In 3D images, the search begins from locations on the medial surface that form junctions on the first slice. Centers of these circles serves as starting points for all possible locations of paths that run in the direction of flow. As shown in the flow chart the algorithm searches for paths starting from centers of circles. For each voxel, the neighbors voxels (18, 26) are found, only voxels that belong to the medial surface are considered a potential voxel in the connected path.

Skeletonization provides an effective image representation by reducing its object dimensionality to a "skeleton" without changing the topology and geometry of the object. An object can be converted to a surface skeleton in 3D (Saha et al., 2015). Skeletonization algorithms perform operations based on a controlled erosion, where the erosion stops when the object thickness becomes 1 or close to 1 ("Morphological operations on binary images"). Skeletonization was used to track the possible paths to measure tortuosity using the MATLAB function bwmorph (BW,'skel',Inf). The operation is set to ‘skel’ and operations are repeated infinitely until the image does not change any more (Bao et al., 2009). The pixels on the boundaries of objects are deleted until no more pixels can be removed where the skeleton of the image is made of the remaining pixels.

3.1.3. Starting Points of Connected Paths

The main goal of this step is to find all possible starting points in the first slice to search for connected paths. The code operates three iterations with connectivity of 8, 4, and 8, respectively. The coordinates for voxel index in the middle of void space and the connected voxels are calculated. In the second iteration, the difference between nodes is calculated to make sure that the movement in voxels is forward. In the third iteration, while loop is implemented to start from id=1 and repeat the calculations until all connected voxel indexes in slide 1 are covered. Temporary position is defined and it is saved as current index if the length of position is greater than 1.

3.1.4. Running the Paths

The code runs the computational steps for each starting points defined in the previous section. In other words, the code finds the next move index for all Path_ID covering the length of Starting_Point_Index. While loop runs as long as the two conditions are satisfied: Next_Move_Index ≠ Size of Image in Directional Flow & Path Corrector =1. The code will find the neighbouring voxels that belong to medial axis surface only. At each step, the code finds the voxel that represents the center of voxels with maximum coordinates in the direction of flow and will save each new voxels as current position. However, if the current voxel (Next_Move_Index) belongs to a solid phase, it will be removed from calculations and the previous position becomes the current position. The code checks the position (solid or void space) at each computational step. These steps will be running for non-connected path until the condition of Path_Corrector does not satisfy and the code checks the next Path_ID. Figure 3.2 shows the flow chart of Running the Path Algorithm.

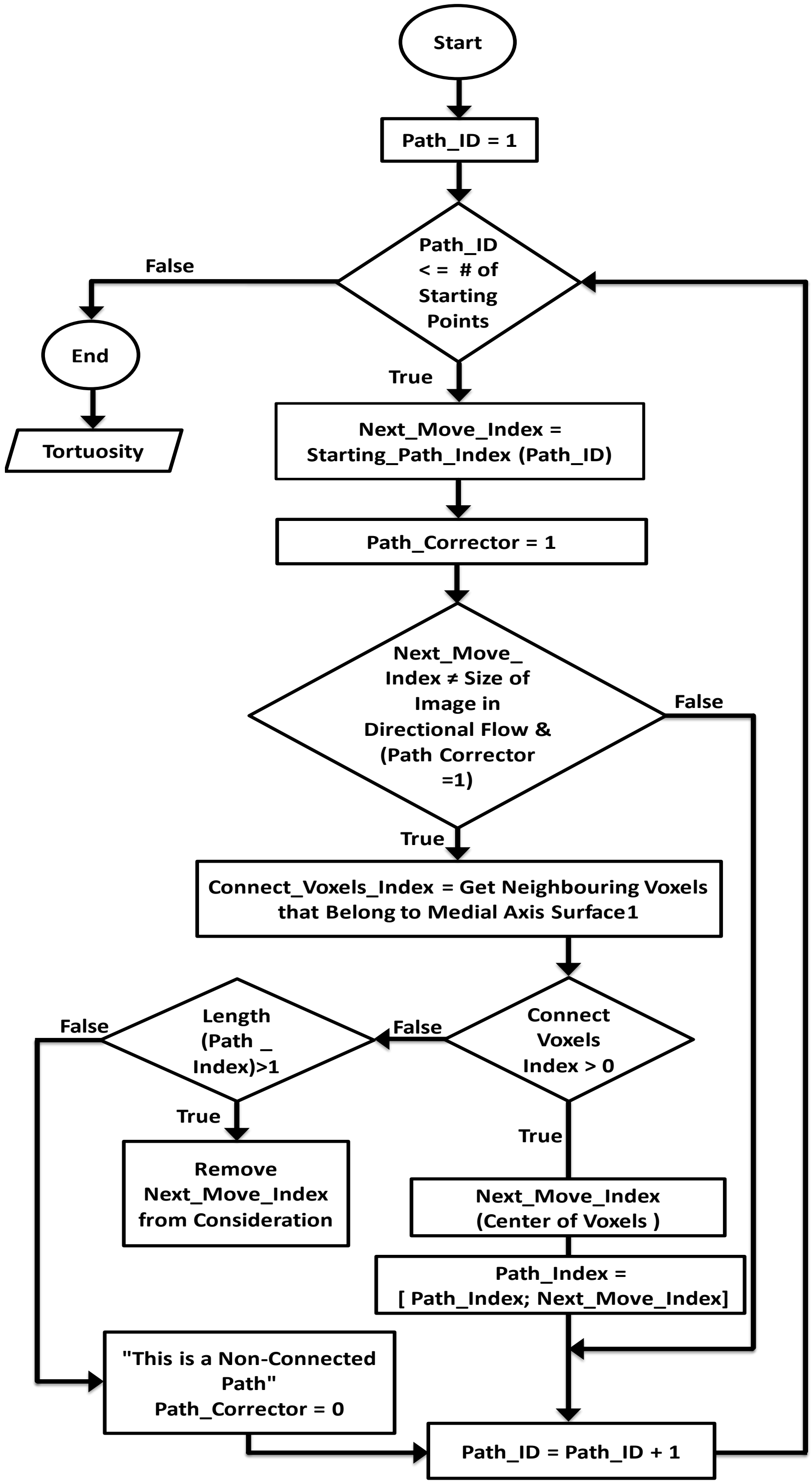

Figure 3.2 Flow Chart of Running the Path Algorithm – Tort3D Code

3.2. Random Paths Code

The key functionality of Random Paths Matlab code is its ability to find tortuosity paths at different specified starting points from 3D images of porous media. The code is simple to use and it needs only to specify limited number of input parameters, such as starting point, number of iterations needed to search for tortuous paths, connectivity, and direction of flow (x , y, or z). In addition, it has been optimized to find out one possible tortuous path in few seconds. Tortuosity for one path can be calculated by dividing the number of voxels needed to reach the first z index equal to the size of the image in the direction of the flow by the size of the image in the direction of the flow. In this work, the size in z direction of the image is 520. The main limitation of the code is its ability to find out only one tortuous path. Identifying large number of paths can take long time to be performed. It can be modified to measure tortuosity for a number of paths instead of one.

The input and output parameters are listed in Table 3.2 and the flow chart of the algorithm is given in Figure 3.2. The algorithm starts by reading segmented binary image. Then, all indices in the void space in the first slice are identified for all possible starting points of tortuous paths. The starting point is selected by specifying the number of element in the list of void indices in the first slice and calculating the x, y, z coordinates of the starting point. Using while loop, the number of iterations needed to identify one possible tortuous path should be specified by the user until the tortuous path is obtained. The 25 connected indices are determined using the existing Matlab code “get_connect_index”. The important part of the code is to check all the connected indices if they are in void phase or solid phase. Then, all the connected indices in the void space that have the highest z index are identified in order to force the movement in z direction. Then, the code is optimized to select one of these indices randomly to be the next move index. The next move index will be the new starting initial point to move in z direction and steps needed to move forward in the path are repeated until the loop is terminated. To identify the number of starting points for possible tortuous paths (i.e. 100 paths), the total number of all indices in the void space in the first slice should be divided by 100 (rounded to nearest integer) and this number should be added to the previous starting point to identify the new starting points for each new tortuous path. The tortuosity (τ) of one path is calculated as:

$$\tau = \frac{N}{D} \qquad \text{(eq. 3.2)}$$

where, N is the number of voxels needed to reach the first index that equals to the size of the image in the direction of flow, and D is the size of the image in the direction of flow, which is 520 in this work. The tortuosity of the 100 paths is the average tortuosity of these paths.

Table 3.2 List of Random Paths Code Inputs and Outputs

	Parameter	Mean
Inputs	raw_image	Segmented image
	initial_position_index	Starting point of tortuous path
	connect	Connectivity type (4,8 in 2D or 6,18,26 in 3D)
	Number of iterations	Number of iterations needed to run to identify one possible tortuous path
Outputs	next_move	x, y, and z coordinates of tortuous path

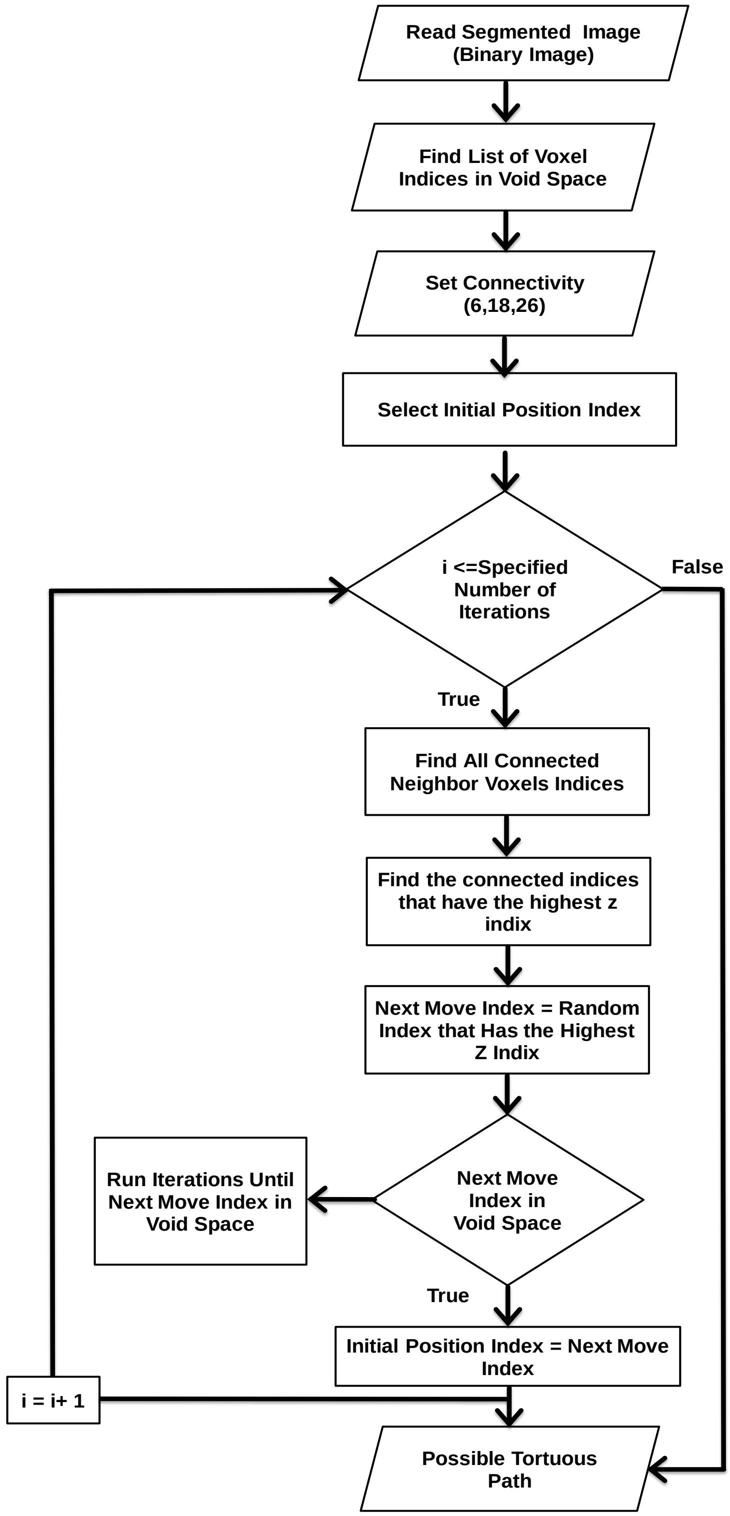

Figure 3.3 Flow Chart of Random Paths Code

3.3. Computed Tomography

X-ray micro-tomography is a powerful technique to visualize the inner structure of porous media. Three-dimensional image is obtained by converting X-ray attenuation data to cross-sections by using image reconstruction algorithms (Al-Raoush, 2014). The sample rotates by specific angle while acquiring the attenuation X-ray. During rotation the X-ray source produces X-rays beam that passes through a section of sample. Detectors are used to register the X-rays that pass through the sample's body as a snapshot in the process of creating an image. During 180° rotation, several snapshots are collected. Then, a computer receives the image data to convert all snapshots to one or multiple cross-sectional images (slices) of the internal structure of the sample (tomographic reconstruction). 3D images are generated from a series of 2D projections taken around a single axis rotation.

3.4. 3D Images Used in the Study

Silica sands, quartz sands, and mixed sands (silica and quartz) were used as porous media (Table 3.3). Sand samples were packed in the aluminum tube under dry conditions to achieve homogeneity (Al-Raoush, 2014). The desired three-dimensional (3D) images of sand samples were acquired by X-ray computed tomography. The details of samples preparation for tomography imaging are explained in Al-Raoush (2014).

The first type of the systems is silica sand, which represent rounded shape. The second type of the systems is quartz sand, which represent angular shape. The third type of the systems is mixed sand, which was created by mixing equal masses of silica and quartz sands. The mixed sand has geometry between rounded and angular geometries. The porosity (∅) of the porous media ranged from 0.32 to 0.49.

Three-dimensional (3D) images of sand systems were acquired by using beamline at the GeoSoilEnviroCARS beamline (13-BM-D) at the Advanced Photon Source, Argonne National Laboratory (Al-Raoush, 2014). Image reconstruction algorithms developed by GSRCARS were used to convert X-ray attenuation data to cross-sections and then to 3D images (Al-Raoush, 2014). Image resolution is 9.6 μm/pixel in all directions. Figure 3.4 shows 2D cross-sections of silica, quartz, and mixed sands from 3D tomography images. Two phases can be easily identified in both images: grains (dark red) and void (dark blue). The size of the images is $380 \times 380 \times 520$ voxels and all the systems achieved the representative elementary volume (REV) for porosity as shown in Figure 3.5 through Figure 3.7.

Table 3.3 Porosity Values of Porous Media

Sand	Silica						Quartz			Mixed			
Porous Media	S1	S2	S3	S4	S5	S6	Q2	Q3	Q6	M1	M2	M3	M4
∅	0.33	0.37	0.33	0.35	0.32	0.38	0.46	0.49	0.49	0.40	0.40	0.39	0.43

∅: Porosity

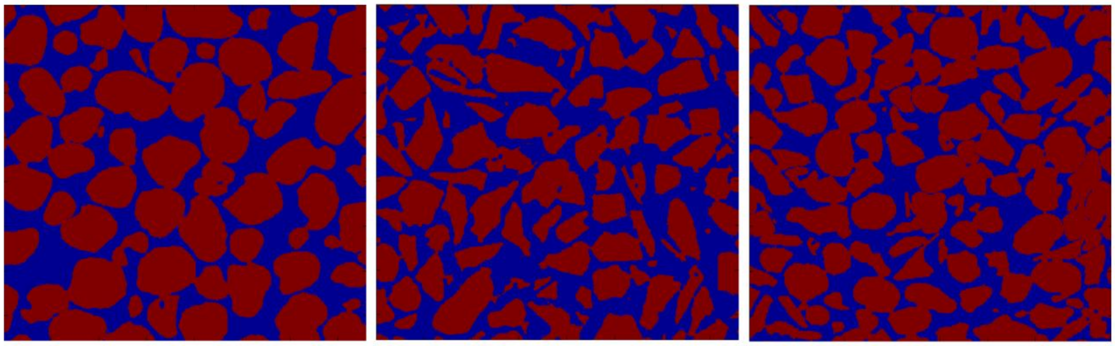

(a) (b) (c)

Figure 3. 4 Cross Sections of Porous Media: (a) Silica Sand, (b) Quartz Sand, (c) Mixed of Silica and Quartz Sands (Al-Raoush, 2014)

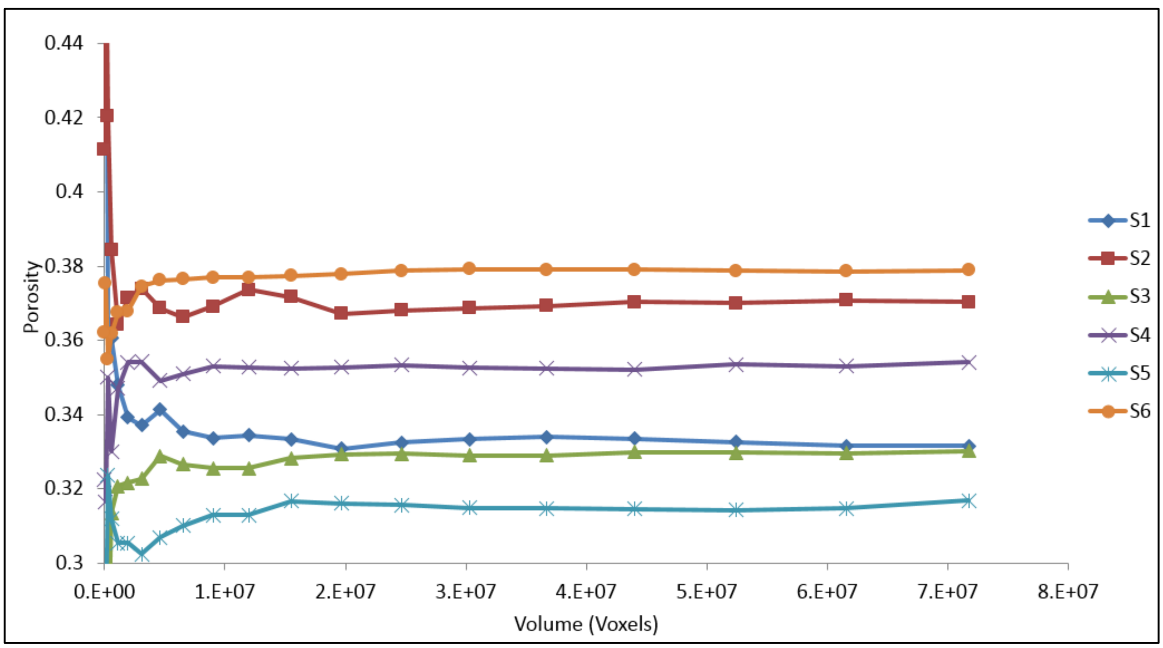

Figure 3.5 REV for Porosity for Silica Sands

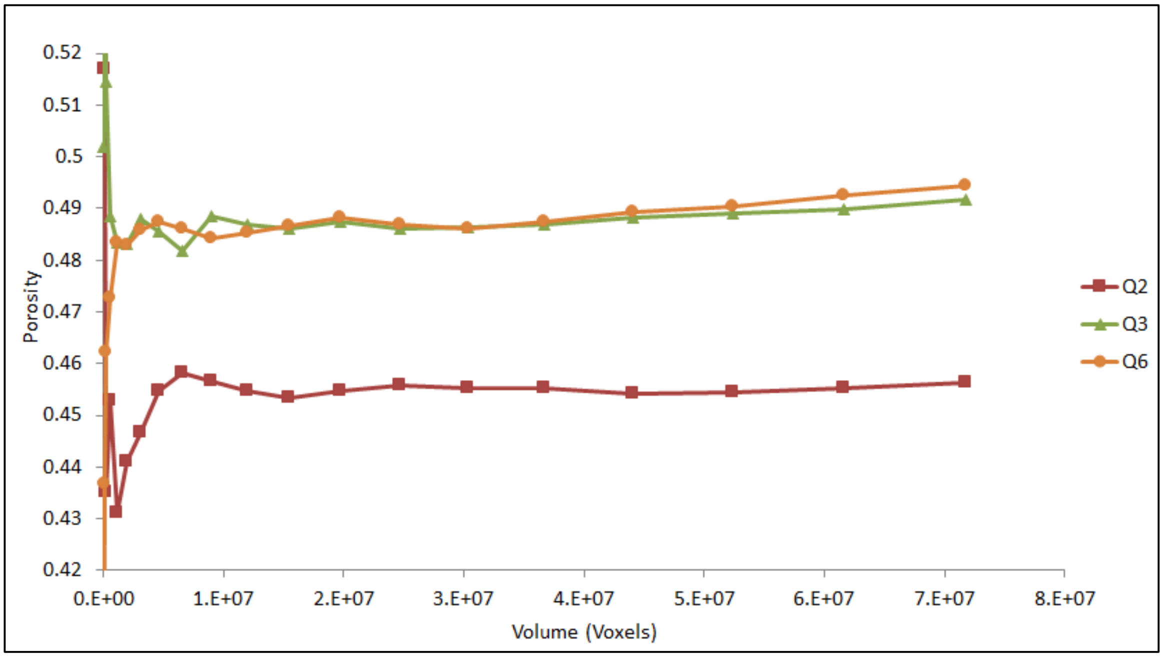

Figure 3.6 REV for Porosity for Quartz Sands

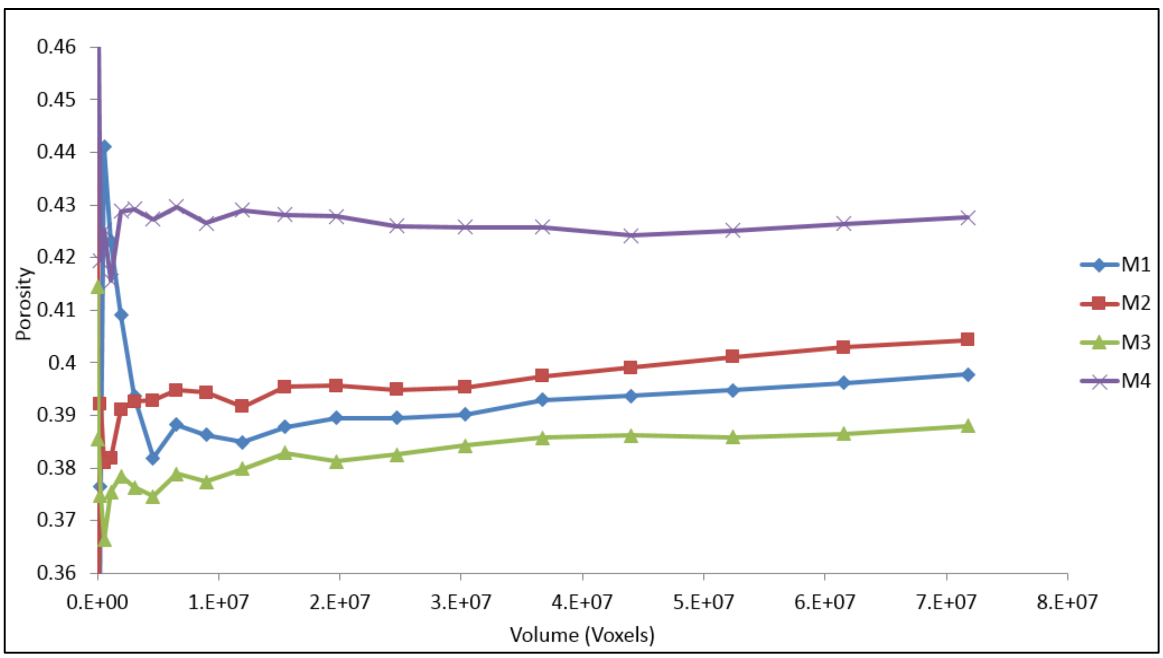

Figure 3.7 REV for Porosity for Mixed Sands

3.5. Image Processing

Image segmentation and calculations of geometrical parameters were performed by Al-Raoush (2014). The explanation of the image processing is given in Appendix A. Physical properties of the systems are listed in Table 3.4. These physical properties are defined as follows:

The coefficient of uniformity (C_u) and The coefficient of gradation (C_c) were computed as:

$$C_u = \frac{d_{60}}{d_{10}} \qquad \text{(e.q. 3.3)}$$

$$C_c = \frac{d_{30}^2}{d_{60}\, d_{10}} \qquad \text{(e.q. 3.4)}$$

Where d_{10} means that 10 percent of the particles are finer and 90 percent of the particles are coarser than that particular particle size d_{10}.

The sphericity index (S_i) describes how closely a grain resembles a sphere, and was computed as follows (Hayakawa and Oguchi, 2005):

$$S_i = \frac{SA_n}{SA_p} \qquad \text{(e.q. 3.5)}$$

Where SA_p is the surface area of the grain and SA_n is the nominal surface area, i.e., the surface area of a sphere having the same volume as the grain. The surface area was computed using a marching tube algorithm. For a perfect sphere, SA_i =1.

The roundness index (R_i) represents the curvature of a grain's corner, was computed as follows:

$$R_i = \frac{3 \times V_p}{SA_p \times D} \qquad \text{(e.q. 3.6)}$$

Where V_p is the volume of the grain and D is the diameter of a grain. The specific surface area (*SSA*) is the ratio of *SA* to the volume.

The mean grain diameter (d_{50}) ranged from 0.18 to 0.43 mm. C_u ranged from 1.52 to 2.49. C_c ranged from 1 to 1.15. S_i ranged from 0.81 to 0.91. R_i ranged from 0.71 to 0.84. The *SSA* ranged from 15.6 to 40.93 mm^{-1}. Porosity values of quartz and mixed sands are higher than these obtained in the silica sands due to difficulty of obtaining dense compactions in systems composed of non-spherical grains. Roundness values of silica sands indicate that the system is composed of highly rounded grains compared with quartz and mixed sands.

Table 3.4 Physical Properties of Studied Porous Media (Al-Raoush, 2014)

Sand	Porous Media	∅	d_{50} (mm)	C_u	C_c	S_i	R_i	*SA* (mm^2)	*SSA* (mm^{-1})
Silica	S1	0.33	0.43	1.86	1.15	0.91	0.84	212.79	15.60
	S2	0.37	0.35	1.85	1.12	0.90	0.83	248.33	19.46
	S3	0.33	0.27	1.79	1.06	0.89	0.81	316.41	23.55
	S4	0.35	0.27	1.79	1.07	0.89	0.81	340.35	26.18
	S5	0.32	0.26	1.83	1.00	0.89	0.82	315.08	22.68
	S6	0.38	0.20	1.52	1.09	0.88	0.81	450.68	36.00
Quartz	Q2	0.46	0.28	2.49	1.06	0.82	0.73	276.85	25.49
	Q3	0.49	0.24	1.95	1.07	0.82	0.71	335.61	32.49
	Q6	0.49	0.18	1.72	1.06	0.81	0.73	406.57	40.93

Table 3.5 Physical Properties of Studied Porous Media (cont.) (Al-Raoush, 2014)

Sand	Porous Media	∅	d_{50} (mm)	C_u	C_c	S_i	R_i	SA (mm^2)	SSA (mm^{-1})
Mixed	M1	0.40	0.30	2.46	1.06	0.84	0.76	274.31	22.83
	M2	0.40	0.25	1.96	1.09	0.85	0.77	341.00	28.68
	M3	0.39	0.23	1.89	1.03	0.86	0.77	345.07	28.47
	M4	0.43	0.19	1.59	1.06	0.85	0.77	434.91	39.25

3.6. Modeling Tortuosity and Geometrical Parameters

Figure 3.8 shows a general flow chart of the steps followed to develop the statistical models of geometrical tortuosity:

- Geometrical tortuosity (using Tort3D code) and porosity were measured using 3D computed tomography images with size 380× 380× 520
- Then, two types of mathematical equations were generated to relate tortuosity with other geometrical parameters:
    - $\tau = b(1)\ \emptyset^{\,b(2)} + b(3)\ d_{50}^{\ b(4)} + b(5)\ C_u^{\ b(6)} + \ldots\ldots..$
    - $\tau = b(1)\ (\emptyset^{\,\wedge b(2)})\ (d_{50}^{\ b(3)})\ (C_u^{\ b(4)})\ldots\ldots..$

where, b(1), b(2), b(3), …, are coefficient parameters calculated in Matlab using Inlinfit function. These types of mathematical equations were selected, since there are many tortuosity models reported in the literature were developed as power law equations (Mota et al., 2001;Coleman and Vassilico, 2008; Nriagu, 1979; Ullman and Aller, 1982; Millington, 1959; van Brakel and Heertjes, 1974)

- Six different tortuosity models as function of geometrical parameters were generated as follows:
    - τ = f($\emptyset$)
    - τ= f($\emptyset$,d_{50})
    - τ = f($\emptyset$,d_{50},C_u,C_c)
    - τ =f($\emptyset$,d_{50},C_u,C_c,SSA)
    - τ =f($\emptyset$,d_{50},C_u,S_i,R_i)
    - τ = f($\emptyset$,d_{50},C_u,C_c,S_i,R_i,SSA)
- A very large number of models were developed for each type of tortuosity models and only the best models were selected and shown in this thesis based on the calculated coefficients, confidence intervals, R^2, and R^2_{adj}
- The predictions of the six developed models were compared based on the R^2, R^2_{adj}, measured tortuosity versus predicted tortuosity, residuals analysis, and sum of squared errors of prediction (SSE)
- The models were validated by comparing predicted tortuosity using developed model (Model 1) and models reported in the literature

The adjusted coefficient of determination (R^2_{adj}) (eq. 3.7) and the sum square error (SSE) (eq.3.8) were used to evaluate the goodness of fit and the accuracy of the estimation, respectively (Cano-Higuitaet al., 2015; Villa-Vélez et al., 2012).

$$R^2_{adj} = 1 - \left(\frac{n-1}{n-n_p-1}\right)(1-R^2) \qquad \text{(eq. 3.7)}$$

$$SSE = \sum_{i=1}^{n}(X_i - X_i^*)^2 \qquad \text{(eq.3.8)}$$

where R^2 and R^2_{adj} are the coefficient of determination and adjusted coefficient of determination between experimental and estimated values by the corresponding model, X_i and X_i* represent the experimental values and the estimated values, n is the number of experimental values and n_p is the number of model parameters.

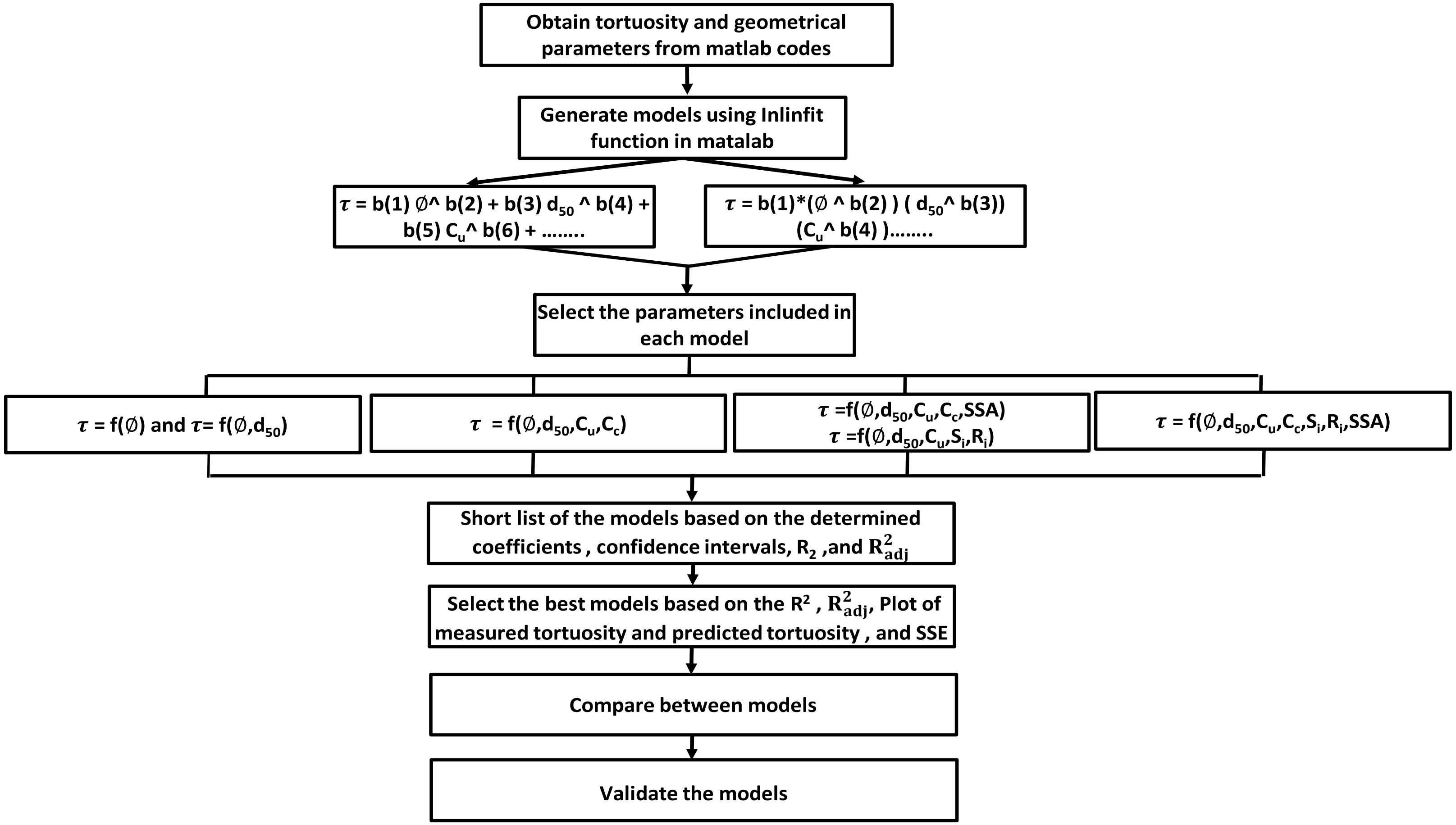

Figure 3.8 Flow Chart of the General Method for Generating Statistical Models of Tortuosity and Other Geometrical Parameters

CHAPTER 4. RESULTS AND DISCUSSION

4.1. Outputs of Tort3D Code

Figure 4.1 shows the centers of these circles, which serve as starting points for all possible locations of paths that run in the direction of flow. The output tortuosity in x and y directions of 2D cross section is shown in Figures 4.2 and 4.3. All 3D paths identified by the code are shown in Figure 4.4. Tortuosity measured by Tor3D code for the 13 systems are presented in Table 4.1. The values ranged from 1.41 to 1.63. Tortuosity values of Quartz and Mixed sands are higher since they have more tortuous paths compared with silica sands.

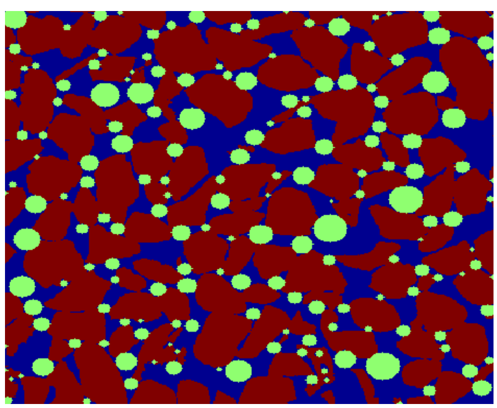

Figure 4.1 Starting Points of the Search for Connected Paths (Green Circles)

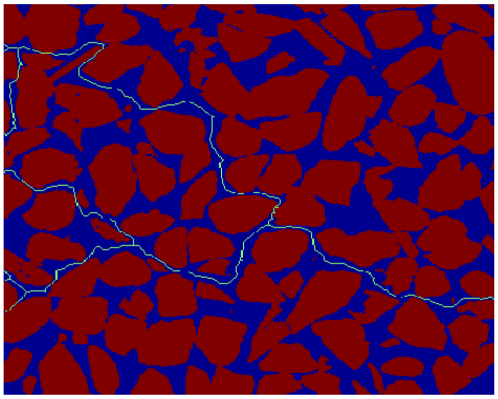

Figure 4. 2 Tortuosity in the X-Direction of 2D Cross Section

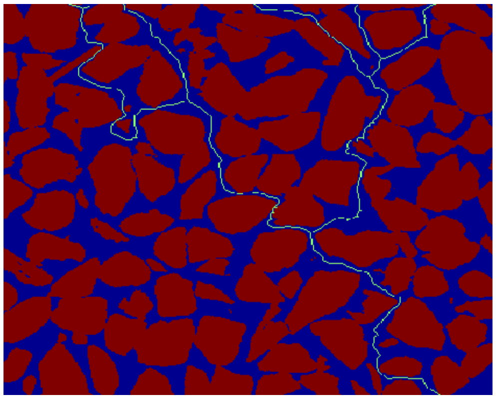

Figure 4.3 Tortuosity in the Y-Direction of 2D Cross Section

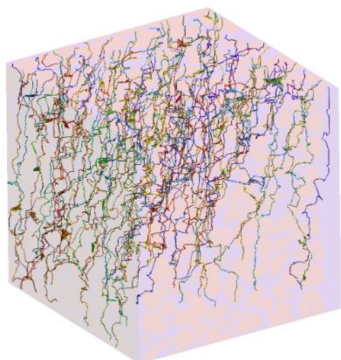

Figure 4.4 3D Tortuous Paths

Table 4.1 Tortuosity Values Measured by Tort3D Code

Sand	Silica						Quartz			Mixed			
Porous Media	S1	S2	S3	S4	S5	S6	Q2	Q3	Q6	M1	M2	M3	M4
τ	1.56	1.46	1.42	1.43	1.51	1.41	1.57	1.63	1.57	1.57	1.56	1.58	1.53

4.2. Tort3D Code Verification

Tort3D was used to measure tortuosity of sand systems to demonstrate the applicability of the code. Reconstructed X-ray CT slices of randomly packed systems made of natural silica and mixed sands were acquired (Figure 4.5). The four systems have different geometrical characteristics (Table 3.4).

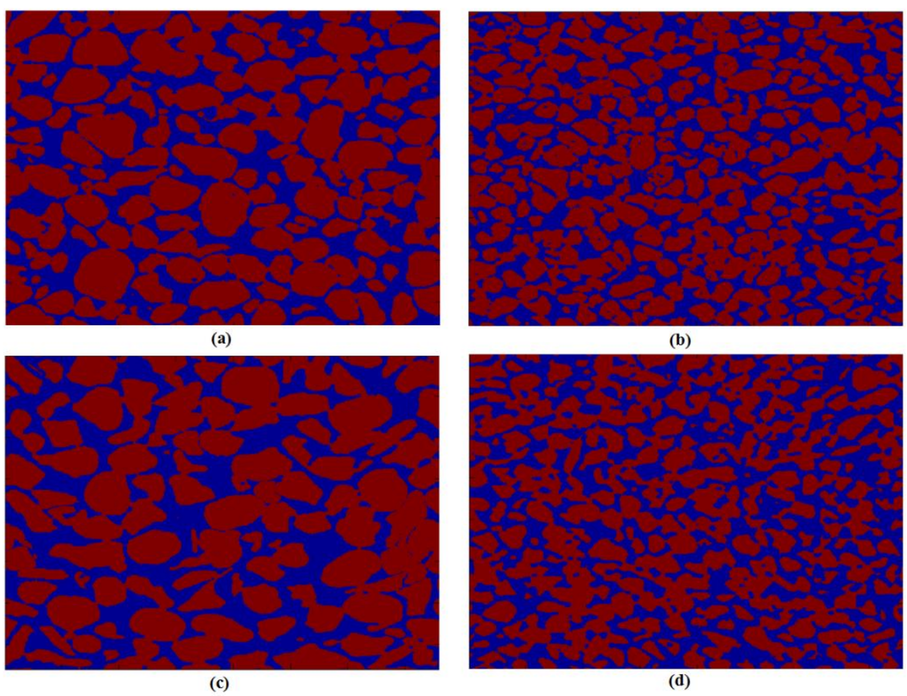

Figure 4.5 Cross Section Image of (a) Silica Sand S5, (b) Silica Sand S6, (c) Mixed Sand M1, and (d) Mixed Sand M4 (Red: Grain Particles, Dark Blue: Void Space (Al-Raoush, 2014)

Measuring tortuosity using Tort3D code does not depend on the geometry of the particles, since tortuosity is measured by summing the length of connected medial axis voxels and dividing them by the straight-line distance. The command "Starting_Paths" is executed to find all possible starting points for connected paths in the first slice. The connected paths determined by the code were 209 and 346 paths for silica and mixed sands, respectively.

Tortuosity values measured by Tort3D code for silica and mixed sands were compared with tortuosity values predicted by models in the literature. These models, their conditions, derivation method, and references are listed in Tables 4.2. Values of predicted tortuosity and difference percentages between measured tortuosity using Tort3D code and predicted tortuosity using models in the literature are reported in Table 4.3. Model 2 was not used for silica sands, since the condition of Model 2 is not applicable for sand system with low porosity value. The same for mixed sands, where the condition of Model 3 does not satisfy. It is apparent that Model 1 and Model 4 give very close tortuosity values for silica sand. Model 4 and Model 5 give very close predictions of tortuosity for the four sand systems.

Table 4.2 Some Tortuosity Models in the Literature

Model#	Model	Condition	Derivation Method	Reference
1	$\tau = 1 - 0.49 \ln\emptyset \quad (\mathrm{eq.\,4.1})$	Bed of sphere, applicable for $0.36 < \emptyset < 1$	Experimental measurement	(Mauret and Renaud, 1997)
2	$\tau = [1 - 0.64(1 - \emptyset)]^{-1} \quad (\mathrm{eq.\,4.2})$	Spherical particles have a low density	Numerical method	(Pisani, 2011)

Table 4.3 Some Tortuosity Models in the Literature (cont.)

Model#	Model	Condition	Derivation Method	Reference
3	$\tau = 1 + 0.64(1 - \emptyset)$ (eq. 4.3)	Spherical particles have a high density	Numerical method	(Pisani, 2011)
4	$\tau = \sqrt{1 + 2(1 - \emptyset)}$ (e. q. 4.4)	Sandy marine sediment, 0.4< $\emptyset$ <0.9	Experimental (diffusion experiment)	(Iversen and Jørgensen, 1993)
5	$\tau = 0.19\, d_{50} + 1.45$ (e. q. 4.5)	Equation derived for Granusil and Accusand sand, which scanned at air-dried and tightly packed conditions using computed tomography analyzer.	Tortuosity values were determined using Medial Axis algorithm in 3DMA-Rock package	(Naveed et al., 2013)

$\emptyset$: Porosity, d_{50}: Median grain diameter (mm)

Referring to Table 4.3 all the models show less than 9% difference except Model 2 for mixed sand M1. For silica sand, the predicted tortuosity using Model 5 is very close to the measured tortuosity with 0.40% difference between the two measurements. This result is expected, since Model 5 was derived from computed tomography data. The low difference obtained using different tortuosity correlations demonstrates that Tort3D code is useful in measuring geometric tortuosity of porous media irrespective of the shape of the system.

Table 4.4 Comparison between Measured Tortuosity using Tort3D Code and Predicted Tortuosity using Models in the Literature

Sand	Tort3D Code	Model1		Model2		Model3		Model4		Model5	
Porous Media	τ	τ	Diff.%	τ	Diff.%	τ	Diff.%	τ	Diff.%	τ	Diff.%
S5	1.51	1.56	3.53	-	-	1.44	4.81	1.54	2.08	1.50	0.40
S6	1.41	1.47	4.50	-	-	1.40	0.81	1.50	5.91	1.49	5.28
M1	1.57	1.45	8.07	1.39	13.2	-	-	1.48	5.67	1.50	4.14
M4	1.53	1.41	8.45	1.57	2.62	-	-	1.46	4.79	1.49	3.22

4.3. Computational Requirements for Tort3D Code

The commands "bwmorph"; "Path_ID"; "Starting_Paths"; and "Tortuosity" were executed and the time needed for the execution was 3:05 minutes for silica sands and 5:55 minutes for mixed sands. The time needed for execution depends on the size of the image and CPU specifications. The images have size of 380×380×520 voxels and the machine used to run the code has the following specification: laptop with processor of 2.5 GHz Intel Core i7, memory of 16 GB DDR3L SDRAM, memory speed of 1600 MHz, and operating system of Windows 8.1. Time for excitation increases as the image size increases, since the image is loaded into memory and it is searched many times to find all possible paths and compute tortuosity. However, the execution time is much shorter than the typical time needed for laboratory experiment (several weeks) (Watanabe and Nakashima, 2002)

4.4. Comparison between Tort3D Code and Random Paths Code

Table 4.4 presents a comparison between Tort3D and Random Paths codes in terms of functionality of the codes, time for processing, efficiency and accuracy, impact of parameters on measuring tortuosity, and limitations.

Table 4.5 Comparison between Tort3D Code and Random Paths Code

	Tort3D Code	Random Paths Code
Function of the Code	Measuring geometrical tortuosity using 3D segmented computed tomography images	Finding out a number of possible random connected paths in void space 3D segmented computed tomography images
Time	Measuring tortuosity takes minutes	Finding out one possible tortuous path in few seconds. Identifying large number of paths can take long time to be performed
Efficiency and accuracy	Measuring tortuosity efficiently and accurately	Identifying tortuous paths efficiently and accurately
Impact of parameters on measuring tortuosity	Measuring tortuosity is slightly influenced by the selected starting points	Measuring tortuosity is influenced by the selected starting points, number of iterations, and number of paths.
Limitations	-	Finding out only one tortuous path. Identifying large number of paths can take long time to be performed

Table 4.5 shows the results of geometrical tortuosity in a certain direction (Z – direction) for the two sand samples analyzed (S5 and M4). It can be observed that the

results are different for the two samples. The lowest values correspond to the Random Paths code. These values seem to be much lower than the values measured by Tort3D code. It can be appreciated scientifically that both codes are based on different concept considering 3D medial surface of the void space (in Tort3D code) and connected voxels in the void space (in Random Paths code).

Table 4.6 Comparison between Tortuosity Values Measured by Tort3D and Random Paths Codes

Sand	Tort3D Code	Random Paths Code	Diff.%
Porous Media	τ	τ	-
Silica Sand S5	1.51	1.15	23.70
Mixed Sand M4	1.53	1.18	22.81

4.5. Modeling of Tortuosity as Function of Geometrical Parameters

Six tortuosity models were generated to relate tortuosity with other geometrical parameters. These models were developed using multiple nonlinear regression analysis. The coefficient parameters in the six models were calculated in Matlab using Inlinfit function. The coefficients were estimated using iterative least squares estimation, with initial values specified by function's element. The first model was developed as a function of $\emptyset$ only and each time one or more geometrical parameters were introduced to the model in order to investigate the significance of the parameters. A very large number of models were developed for each type of tortuosity models. The models that have unrealistic power values were eliminated and only the best models were selected and shown in this thesis. The predictions of the six developed models were compared based on the validation criteria described below.

4.5.1. Relation between Tortuosity and Porosity

The first developed model is Model 1, which relates tortuosity to porosity as follows:

$$\tau = \emptyset^2 + 1.3562 \qquad \text{(e.q. 4.6)}$$

Figure 4.6 (a) shows a plot of linear correlation between measured tortuosity and predicted tortuosity. It is seen that 5 measurements fall no far away from the perfect line, which indicates that the predicted tortuosity from validation does not have very good correlation with the measured tortuosity. Figure 4.7 (a) shows a plot of residual on the y axis and fitted values of tortuosity appear on x axis. The residuals ranged between -0.08 and 0.08. The residuals roughly do not form a "horizontal band" around 0 line, which indicates that the variances of the error are not equal. Some residuals do not follow the random pattern of residuals showing outliners. Figure 4.8 (a) shows a normal probability plot of residuals. The plot looks fairly straight, when the large and small results are ignored. These results are likely outliners.

A shown in Table 4.6, the coefficient of determination (R^2) is 0.405 and the adjusted coefficient of determination (R^2_{adj}) is 0.351, which indicate unacceptable correlation has been reached from this set of tortuosity values. By examining the sum square error (SSE) (0.037) and the maximum error (6.702%), the two values are low. However, the low values of R^2 and R^2_{adj}, measured tortuosity versus predicted tortuosity, residuals, and normal probability of residuals indicate that porosity is not the only factor that influence tortuosity. The following sections investigate the relationships between tortuosity and other geometrical parameters.

4.5.2. Model of Tortuosity as a Function of Porosity and Median Particle Diameter

In the second model, median particle diameter, d_{50}, has been introduced in the model to study its influence on tortuous flow path as follows:

$$\tau = 1.3081\ \emptyset^{1.9982} + 1.058\ d_{50}^{0.1514} + 0.4523 \qquad \text{(e.q. 4.7)}$$

Referring to Figure 4.6 (b), approximately half of the values spread close to the perfect fitting line. In Figure 4.7 (b) the residuals are not distributed equally showing that the variances are not constant. As shown in Figure 4.8 (b), most of the residual points fall in the straight line except the large and small residual points.

According to e.q. 4.8, the porosity, $\emptyset$, has more effect on tortuosity than the median particle diameter, d_{50}, which indicates less contribution in the model. As shown in Table 4.6, R^2 R^2_{adj} increased to 0.536 and 0.443, respectively. The SSE and maximum error percentage are low. However, the values of R^2 and R^2_{adj} are not high enough to make the proposed model predicts tortuosity values accurately. The results of validating the model show that the model cannot predict tortuosity values accurately for different porous systems and investigation of other models is needed.

4.5.3. Model of Tortuosity as a Function of Porosity, Median Particle Diameter, Uniformity Coefficient, and Coefficient of Gradation

In Model 3, uniformity coefficient, C_u, and coefficient of gradation, C_c, were taken into consideration by adding these two parameters to $\emptyset$, and d_{50} (the most prominent parameter in the model) as follows:

$$\tau = 1.77\ \emptyset^{0.4377} + d_{50}^{1.8667} + 0.1861\ C_u^{0.2703} + 0.1615\ C_c^{-26.3848} \qquad \text{(e. q. 4.8)}$$

In Figure 4.6 (c), majority of data points are clustered close to the perfect fitting line. The measured tortuosity versus predicted tortuosity for Model 3 shows better prediction than the plots of the other models. Figure 4.7 (c) shows scatter plot of residuals of Model 3. The residuals scatter more uniformity than the residuals of Models 1 and 2. Figure 4.8 (c) shows that residuals are approximately normally distributed. According to Table 4.6, the model has acceptable R^2 (0.749) and R_{adj}^2 (0.623). These values are the highest compared to those values for other models. Also, SSE and maximum error percentage are the lowest values obtained for the model. All the validation results show that Model 3 has the best prediction capability.

4.5.4. Model of Tortuosity as a Function of Porosity, Median Particle Diameter, Uniformity Coefficient, Coefficient of Gradation, and Roundness Index

Model 4 includes roundness index, R_i, in addition to the parameters of Model 3 ($\emptyset$, d_{50}, C_u, C_c) as follows:

$$\tau = 0.7716\ \emptyset + 2.8314\ d_{50} + 0.0348\ C_u - 1.9771\ C_c + 1.3043\ R_i^{0.1998} \qquad \text{(e. q. 4.9)}$$

The addition of roundness index affects the capability of the model in predicting tortuosity. The most prominent parameter is d_{50}. The data points in Figure 4.6 (d) are not well clustered around the perfect fitting line. In Figure 4.7 (d), the residuals are scattered roughly around zero line. However, the normal probability plot of residuals shows a normal distribution of residuals, when the last point is ignored. According to Table 4.6, adding R_i in the model leads to decrease R^2 and R^2_{adj} to 0.710 and 0.504. However, SSE and maximum error percentage are still low.

4.5.5. *Tortuosity as a Function of Porosity, Median Particle Diameter, Uniformity Coefficient, Spherecity Index, and Roundness Index*

Model 5 shows another type of correlation of tortuosity with different geometrical parameters ($\emptyset$, d_{50}, C_u,, S_i, R_i) as follows:

$$\tau = \frac{1.2902\ d_{50}^{0.244}}{\emptyset^{0.2518}\ C_u^{0.2996}\ S_i^{2.1859}\ R_i^{0.5062}} \qquad \text{(e.q. 4.10)}$$

Figure 4.6 (e) does not show a good correlation for predicting tortuosity, since the data points are not clustered uniformly around the perfect fitting line. Figure 4.7 (e) approximately shows S shape that the data are not uniformly distributed. According to Table 4.6, R^2 is still high (0.708) but R^2_{adj} is considered low (0.500). SSE and maximum error percentage of Model 5 are similar to the values obtained for Model 4.

4.5.6. Model Tortuosity as a Function of All Geometrical Parameters

Model 6 considers the effects of all geometrical parameters in the study ($\emptyset$, d_{50}, C_u, C_c, S_i, R_i, SSA) as follows:

$$\tau = \frac{13.1187\, d_{50}^{0.0319}}{\emptyset^{0.0111}\, C_u^{0.0402}\, C_c^{0.0446}\, S_i^{0.2703}\, R^{0.0231}\, SSA^{0.004}} - 11.2264 \qquad \text{(e.q. 4.11)}$$

The contribution of each parameter is very low according to their power values. The combination of all parameters affects their real effect on tortuous path length. Figure 4.6 (f) does show good correlation between measured tortuosity and predicted tortuosity. Also, the residuals are not scattered uniformly as shown in Figure 4.7 (f). The data points form relatively a straight line, when the residuals ranged between -0.055 and 0.04. The 95% confidence interval has a very large range. Even SSE and maximum error percentages are low, the R_{adj}^2 (0.357) is very low compare to R^2 (0.732), which indicates that the model cannot predict real tortuosity values.

Table 4.7 shows a comparison between all models and scoring them for each validation criteria. The higher number assigned to the model, the better model capability for predicting tortuosity. According to the table, Model 3 has the highest score compared to other models and it is the best model that can predict tortuosity values accurately.

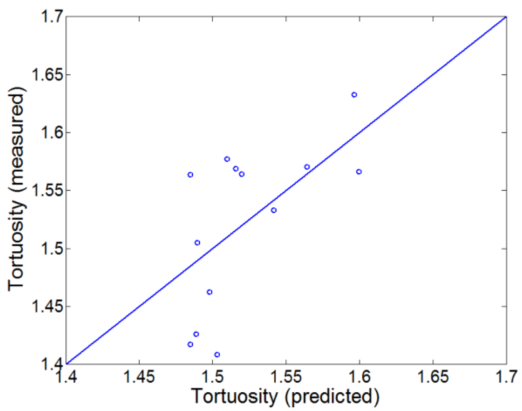

(a) Model 1

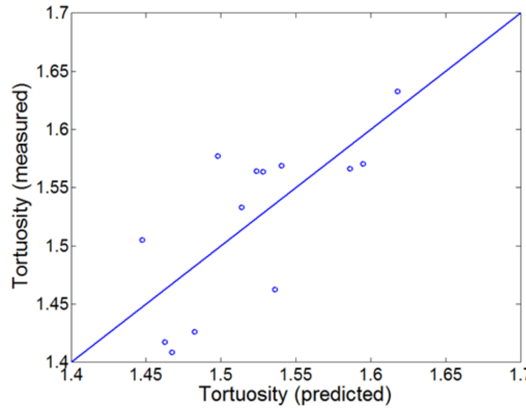

(b) Model 2

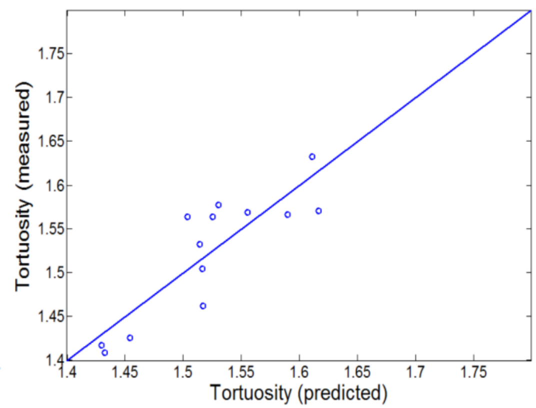

(c) Model 3

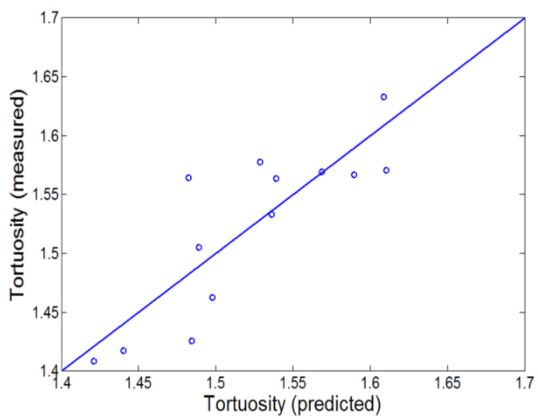

(d) Model 4

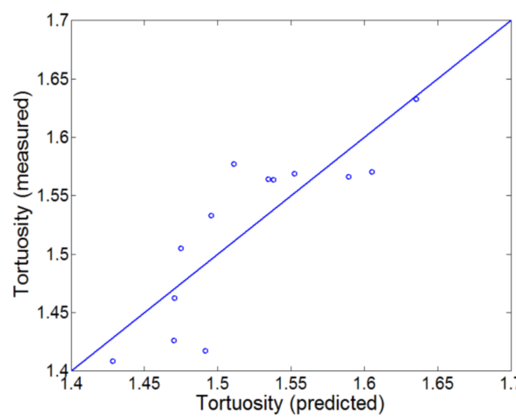

(e) Model 5

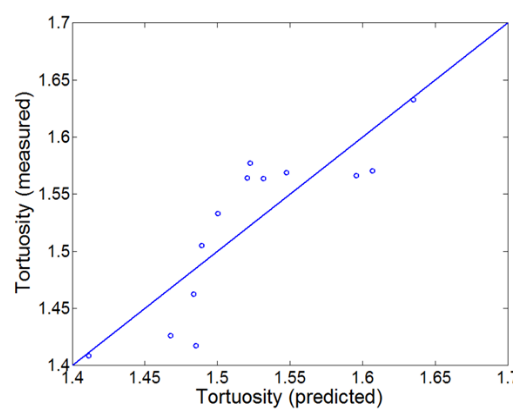

(f) Model 6

Figure 4.6 Measured Tortuosity versus Predicted Tortuosity

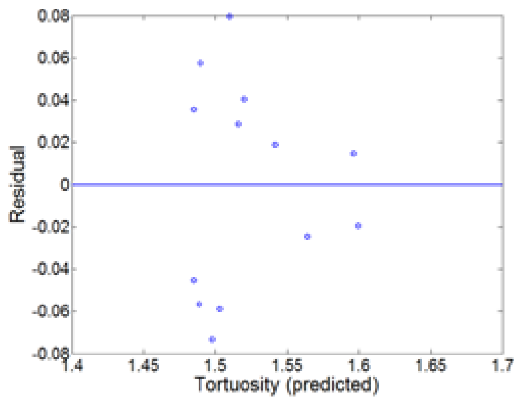

(a) Model 1

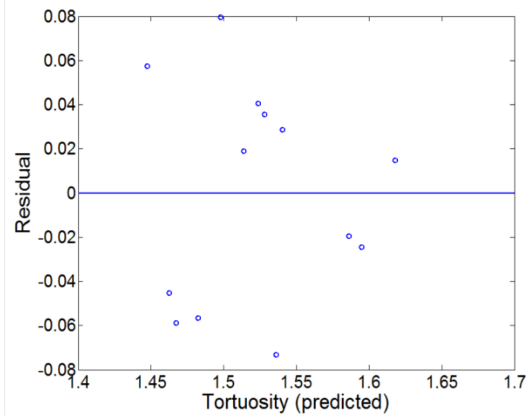

(b) Model 2

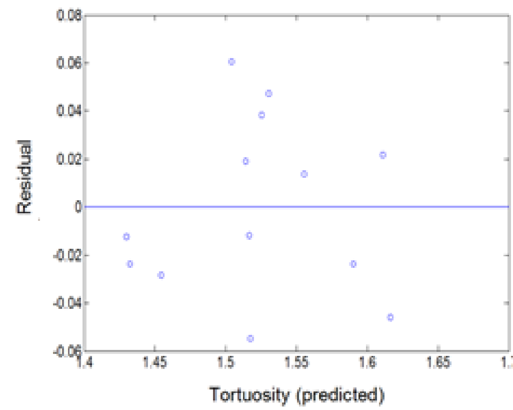

(c) Model 3

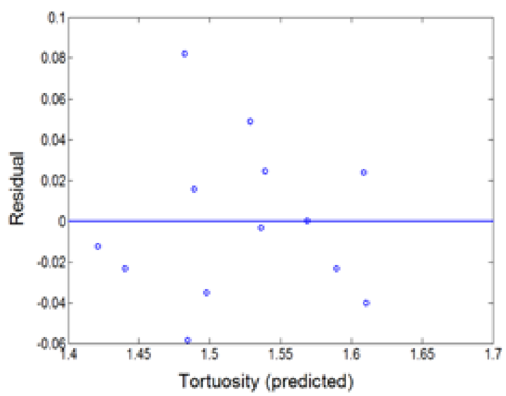

(d) Model 4

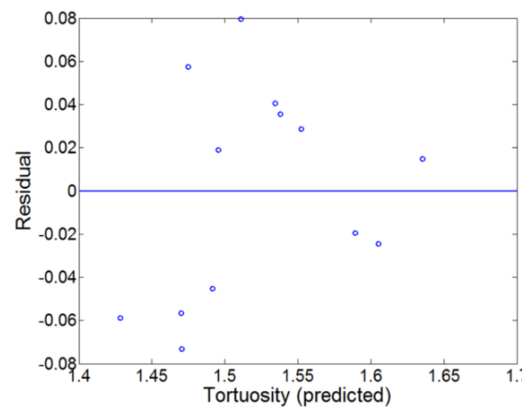

(e) Model 5

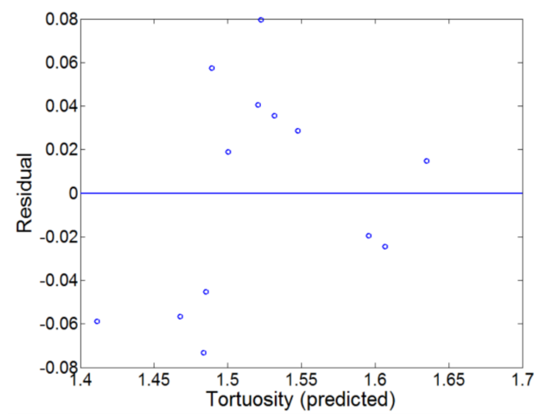

(f) Model 6

Figure 4.7 Residual versus Predicted Tortuosity

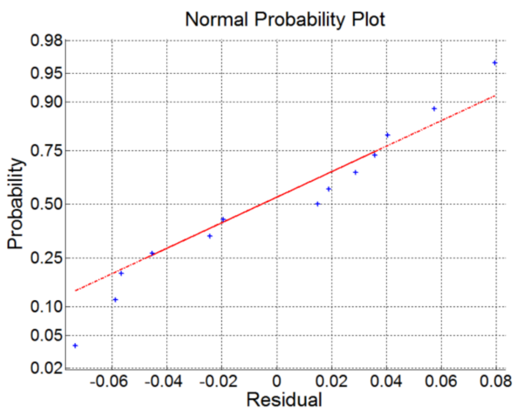

(a) Model 1

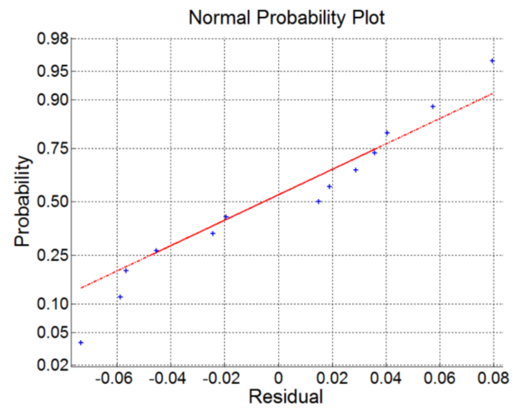

(b) Model 2

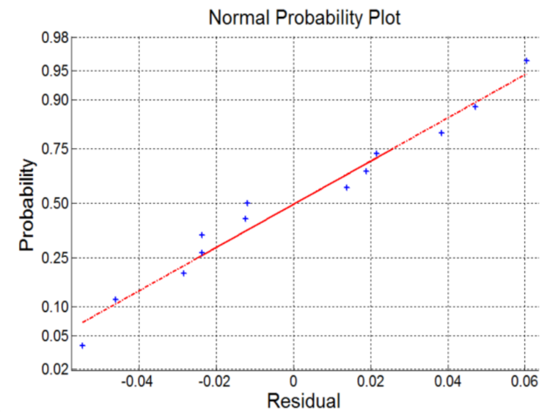

(c) Model 3

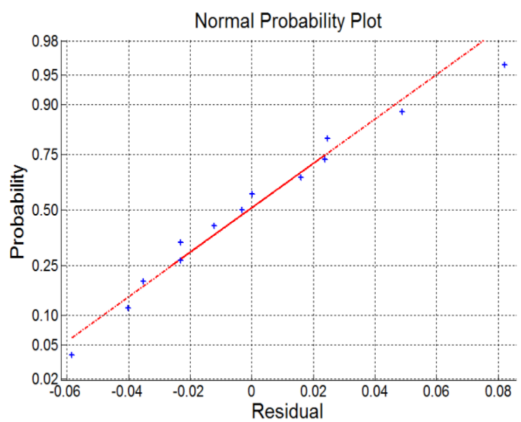

(d) Model 4

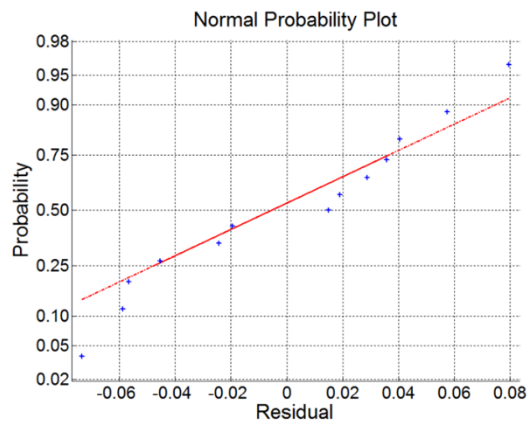

(e) Model 5

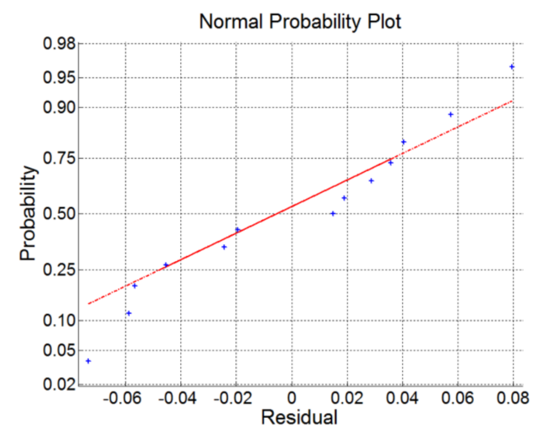

(f) Model 6

Figure 4.8 Normal Probability of Residual

Table 4.7 Parameter Results from Modelling of Tortuosity

Model#	Model	C.I (95%)	R^2	R^2_{adj}	SSE	Error $_{minimum}$%	Error $_{maximum}$%
1	$\tau = \emptyset^2 + 1.3562$ (e.q. 4.7)	-0.0000 0.0000 -156.5413 128.8287 1.2912 1.4213	0.4054	0.351345	0.037132	0.401172	6.70169
2	$\tau = 1.3081\ \emptyset^{1.9982} + 1.058\ d_{50}^{0.1514} + 0.4523$ (e.q. 4.8)	-3.9970 6.6133 -8.3453 12.3416 -41.5820 43.6981 -7.9078 8.2107 -43.0240 43.9286	0.5355	0.4426	0.028992	0.912599	5.03962
3	$\tau = 1.77\ \emptyset^{0.4377} + d_{50}^{1.8667} + 0.1861\ C_u^{0.2703} + 0.1615\ C_c^{-26.3848}$ (e.q. 4.9)	-18.4366 21.9767 -7.4414 8.3168 -2.0769 5.8102 -21.6869 22.0590 -25.4248 25.9655 -0.1629 0.4858 -139.3504 86.5808	0.7485	0.62275	0.015697	0.784053	3.867297
4	$\tau = 0.7716\ \emptyset + 2.8314\ d_{50} + 0.0348\ C_u - 1.9771\ C_c + 1.3043\ R_i^{0.1998}$ (e.q. 4.10)	-0.9770 2.5202 -1.2390 6.9018 -0.2124 0.2820 -4.4797 0.5256 -0.3781 2.9868 -0.1722 0.5718	0.7104	0.503543	0.018068	0.006373	5.254411

Table 4.8 Parameter Results from Modelling of Tortuosity (cont.)

Model#	Model	C.I (95%)	R^2	R^2_{adj}	SSE	Error $_{minimum}$%	Error $_{maximum}$%
5	$\tau = \frac{1.2902\ d_{50}^{0.244}}{\emptyset^{0.2518}\ C_u^{0.2996}\ S_i^{2.1859}\ R_i^{0.5062}}$ (e.q. 4.11)	0.2631 2.3174 -0.8950 0.3914 -0.1172 0.6052 -0.8834 0.2841 -9.9455 5.5736 -4.8116 3.7991	0.7083	0.499943	0.018188	0.159245	5.242362
6	$\tau = \frac{13.1187\ d_{50}^{0.0319}}{\emptyset^{0.0111}\ C_u^{0.0402}\ C_c^{0.0446}\ S_i^{0.2703}\ R^{0.0231}\ SSA^{0.004}} - 11.2264$ (e.q. 4.12)	1.0e+003 * -7.9733 7.9995 -0.0071 0.0071 -0.0204 0.0205 -0.0256 0.0256 -0.0287 0.0286 -0.1742 0.1736 -0.0133 0.0132 -0.0024 0.0024 -8.0010 7.9785	0.7322	0.35728	0.01671	0.134746	4.790799

Table 4.9 Comparison Between All Developed Tortuosity Models

	Measured Tortuosity versus Predicted Tortuosity	Residuals Plot	Normal Probability Plot	R^2	R^2_{adj}	SSE	Error $_{minimum}$%	Error $_{maximum}$%	Total	Rank
Model 1	3	1	4	2	2	4	5	4	25	5
Model 2	3	1	4	3	3	4	4	4	26	6
Model 3	5	3	5	5	4	5	4	6	37	1
Model 4	4	3	5	4	3	4	6	5	34	2
Model 5	4	2	4	4	3	4	5	5	31	3
Model 6	4	2	4	4	2	4	5	5	30	4

5: Very good, 4: Good, 3: Fair,2: Poor, 1: Very poor

4.5.7. Model Validation

According to the results of the previous section, relating geometrical tortuosity to $\emptyset$, d_{50}, C_u, and C_c gives better predictions of tortuosity. Most of the tortuosity models in the literature are functions of $\emptyset$ or d_{50} only. Predictions of developed Model 1 ($\tau = \emptyset^2 + 1.3562$) have been compared to the predictions of models in the literature that were used for Tort3d code verification (listed in the Table 4.2). The difference percentages obtained for Model 1 (developed) are lower than those obtained for Models 1, 3, and 5 for ten samples (except S1, S2, S6; S3, S4, S6; S1, S5, S6) and 11 samples (except S1, S6) for Model 4. Model 1 (developed) predicts tortuosity better than Model 2 (literature) for all samples. The results show that Model 1 (developed) has better capability to predict tortuosity. A shown in Table 4.8 and explained in the previous sections that developed models (Model 2, Model 3, Model 4, Model 5, Model 6) in this study give better predictions of tortuosity. These models can measure tortuosity better than those models reported in the literature. That proves that Model 3 is the best model.

Table 4.8 Difference percentage between Measured Tortuosity and Predicted Tortuosity by Developed Model 1 and Models in the Literature

Sand	Difference %					
Porous Media	Model 1 (Developed)	(e.q. 4.1)	(e.q. 4.2)	(e.q. 4.3)	(e.q. 4.4)	(e.q. 4.5)
S1	5.06	1.43	11.81	8.68	2.23	2.02
S2	2.41	1.59	14.44	4.11	2.74	3.71
S3	4.78	8.94	23.59	0.83	7.95	5.93
S4	4.41	5.85	19.61	0.86	6.19	5.24
S5	1.02	3.66	17.79	4.59	2.12	0.40
S6	6.70	4.72	17.78	0.81	6.29	5.58

Table 4.8 Difference percentage between Measured Tortuosity and Predicted Tortuosity by Developed Model 1 and Models in the Literature (cont.)

Sand	Difference %					
Porous Media	Model 1 (Developed)	(e.q. 4.1)	(e.q. 4.2)	(e.q. 4.3)	(e.q. 4.4)	(e.q. 4.5)
Q2	0.40	11.80	2.28	14.14	7.97	4.33
Q3	2.22	17.35	9.08	18.76	12.95	8.43
Q6	2.11	14.07	5.53	15.47	9.43	5.28
M1	3.40	7.47	3.72	11.70	5.37	3.98
M2	2.85	7.60	3.46	11.65	5.31	4.25
M3	4.29	7.30	4.07	11.83	5.52	5.31
M4	0.57	7.79	2.69	10.97	4.57	3.12

CHAPTER 5. CONCLUSIONS

The thesis presented Tort3D code (existing code) to measure geometric tortuosity from segmented binary X-ray images of porous media. X-ray computed tomography imaging was used to construct 3D high resolution images of 13 natural sand systems. The code was developed in MATLAB to read segmented binary image and find out all possible tortuous paths in a porous media system. Geometric tortuosity was measured for silica, quartz, and mixed sands with time less than 6 minutes. The measured tortuosity values were compared with predicted values by models in the literature and low difference percentages were obtained. The results demonstrated that the code can successfully measure geometric tortuosity for any porous system irrespective of the shape of the materials. Another code that was developed in this study is named Random Paths code. It was developed on a concept of measuring tortuosity in any connected path in the void space in very few seconds. The main limitation of this code is measuring tortuosity for one path only. Measuring tortuosity for a number of paths needs to be done manually. Tortuosity values measured by Tort3D and Random Paths codes were different, since the two codes are based on different concepts.

Also, the thesis included modeling tortuosity (measured by Tort3D code) as a function of geometrical parameters for 13 soil samples with an aim to examine the effect of adding parameter(s) to each model on the capability of the model to predict accurate tortuosity values. Based on the findings of the modeling, the following conclusions are drawn:

- The combination of $\emptyset$, d_{50}, C_u, and C_c has a significant impact on tortuosity.
- Model 3 has the best capability to predict tortuosity for different porous systems based on the statistical analysis
- The study shows considering all the geometrical parameters in one model can reduce their ability to predict tortuosity.
- Further study regarding modeling tortuosity with other geometrical parameters for materials with different properties is necessary.

References

Adler, P. M. (1992). Porous media: Geometry and transports. Butterworth–Heinemann. Stoneham.

Ahmadi, M. M., Mohammadi, S., and Hayati, A. N. (2011). Analytical derivation of tortuosity and permeability of monosized spheres: A volume averaging approach. *Physical Review E - Statistical, Nonlinear, and Soft Matter Physics*, *83*(2). doi:10.1103/PhysRevE.83.026312

Akanni, K. A., Evans, J. W., and Abramson, I. S. (1987). Effective transport coefficients in heterogeneous media. *Chemical Engineering Science*, *42*(8), 1945-1954. doi:http://dx.doi.org/10.1016/0009-2509(87)80141-0

Al-Arif, S., Ferdous, A., and Nijami, S. (2012). Comparative Study of Different Path Planning Algorithms: A Water based Rescue System. *International Journal of Computer Applications*, *39*.

Al-Raoush, R. I. (2014). Experimental investigation of the influence of grain geometry on residual NAPL using synchrotron microtomography. *Journal of Contaminant Hydrology*, *159*, 1-10. doi:10.1016/j.jconhyd.2014.01.008

Androutsopoulos, G. P., and Salmas, C. E. (2000). Tomography of macro-meso-pore structure based on mercury porosimetry hysteresis loop scanning. Part I: MP hysteresis loop scanning along the overall penetration line. *Chemical Engineering Communications*, *181*, 137-177.

Ballal, G., and Zygourakis, K. (1985). Diffusion in particles with pores of varying cross-section. *Chemical Engineering Science, 40*(8), 1477-1483. doi:10.1016/0009-2509(85)80089-0

Bao, M., Guo, S., Tang, Q., and Zhang, F. (2009). *Optimization of the bwmorph Function in the MATLAB image processing toolbox for binary skeleton computation.* Paper presented at the Proceedings of the 2009 International Conference on Computational Intelligence and Natural Computing, CINC 2009.

Bear, J. (1972). Dynamics of fluids in porous media. New York: American Elsevier Pub. Co.

Bhatia, S. K. (1985). Directional autocorrelation and the diffusional tortuosity of capillary porous media. *Journal of Catalysis, 93*(1), 192-196. doi:10.1016/0021-9517(85)90163-0

Boudreau, B. P. (1996). The diffusive tortuosity of fine-grained unlithified sediments. *Geochimica et Cosmochimica Acta, 60*(16), 3139-3142. doi:http://dx.doi.org/10.1016/0016-7037(96)00158-5

Cano-Higuita, D. M., Villa-Vélez, H. A., Telis-Romero, J., Váquiro, H. A., and Telis, V. R. N. (2015). Influence of alternative drying aids on water sorption of spray dried mango mix powders: A thermodynamic approach. *Food and Bioproducts Processing, 93*, 19-28. doi:10.1016/j.fbp.2013.10.005

Childs, E. C. (1969). An introduction to the physical basis of soil water phenomena. New York: Wiley-Interscience.

Chung, S. Y., Han, T. S., and Kim, S. Y. (2015). Reconstruction and evaluation of the air permeability of a cement paste specimen with a void distribution gradient using CT images and numerical methods. *Construction and Building Materials, 87*, 45-53. doi:10.1016/j.conbuildmat.2015.03.103

Civan, F. (2010). Effective correlation of apparent gas permeability in tight porous media. *Transport in Porous Media, 82*(2), 375-384. doi:10.1007/s11242-009-9432-z

Clennell, M. B. (1997) Tortuosity: a guide through the maze. *Vol. 122. Geological Society Special Publication* (pp. 299-344).

Coleman, S. W., and Vassilicos, J. C. (2008). Transport properties of saturated and unsaturated porous fractal materials. *Physical Review Letters, 100*(3). doi:10.1103/PhysRevLett.100.035504

Comiti, J., and Renaud, M. (1989). A new model for determining mean structure parameters of fixed beds from pressure drop measurements: application to beds packed with parallelepipedal particles. *Chemical Engineering Science, 44*(7), 1539-1545. doi:10.1016/0009-2509(89)80031-4

Cornea, N. D., Silver, D., and Min, P. (2007). Curve-skeleton properties, applications, and algorithms. *IEEE Transactions on Visualization and Computer Graphics, 13*(3), 530-548. doi:10.1109/TVCG.2007.1002

Corrochano, B. R., Melrose, J. R., Bentley, A. C., Fryer, P. J., and Bakalis, S. (2014). A new methodology to estimate the steady-state permeability of roast and ground coffee in packed beds. *Journal of Food Engineering, 150*, 106-116. doi:10.1016/j.jfoodeng.2014.11.006

Dechter, R., and Pearl, J. (1985). GENERALIZED BEST-FIRST SEARCH STRATEGIES AND THE OPTIMALITY OF A*. *Journal of the ACM, 32*(3), 505-536. doi:10.1145/3828.3830

Dijkstra, E. (1959). A Note on Two Problems in Connexion with Graphs.

Dijkstra's algorithm , Bellman Ford algorithm , Single-source shortest paths ; Dijkstra algoritması nedir - Bellman Ford algoritması nedir. (2014). Retrieved from http://omeriyioz.blogspot.qa/2014/01/dijkstras-algorithm-shortest-path-for.html

Du Plessis, J. P., and Masliyah, J. H. (1991). Flow through isotropic granular porous media. *Transport in Porous Media, 6*(3), 207-221. doi:10.1007/BF00208950

Duda, A., Koza, Z., & Matyka, M. (2014). Hydraulic tortuosity in arbitrary porous media flow. *Physical Review E - Statistical, Nonlinear, and Soft Matter Physics, 84*(3). doi:10.1103/PhysRevE.84.036319

Dykhuizen, R. C., and Casey, W. H. (1989). An analysis of solute diffusion in rocks. *Geochimica et Cosmochimica Acta, 53*(11), 2797-2805. doi:10.1016/0016-7037(89)90157-9

Feller, C., Schouller, E., Thomas, F., Rouiller, J., and Herbillon, A. J. (1992). N<inf>2</inf>-bet specific surface areas of some low activity clay soils and their relationships with secondary constituents and organic matter contents. *Soil Science, 153*(4), 293-299.

Feng, C., Zhao, D., and Huang, M. (2016). Segmentation of longitudinal brain MR images using bias correction embedded fuzzy c-means with non-locally spatio-temporal regularization. *Journal of Visual Communication and Image Representation, 38*, 517-529. doi:10.1016/j.jvcir.2016.03.027

Feng, Y., Yu, B., Zou, M., and Xu, P. (2007). A generalized model for the effective thermal conductivity of unsaturated porous media Based on self-similarity. *Journal of Porous Media, 10*(6), 551-567. doi:10.1615/JPorMedia.v10.i6.30

Gao, X., Diniz da Costa, J. C., and Bhatia, S. K. (2014). Understanding the diffusional tortuosity of porous materials: An effective medium theory perspective. *Chemical Engineering Science, 110*, 55-71. doi:10.1016/j.ces.2013.09.050

Ghanbarian, B., Hunt, A. G., Ewing, R. P., and Sahimi, M. (2013). Tortuosity in porous media: A critical review. *Soil Science Society of America Journal*, *77*(5), 1461-1477. doi:10.2136/sssaj2012.0435

Grathwohl, P. (1998). Diffusion in Natural Porous Media: Contaminant Transport, Sorption/Desorption and Dissolution Kinetics. Boston: Kluwer Academic Publishing.

Guo, J., Quintard, M., and Laouafa, F. (2015). Dispersion in Porous Media with Heterogeneous Nonlinear Reactions. *Transport in Porous Media, 109*(3), 541-570. doi:10.1007/s11242-015-0535-4

Guéguen, L. (2001) Segmentation by maximal predictive partitioning according to composition biases. *Vol. 2066. Lecture Notes in Computer Science (including subseries Lecture Notes in Artificial Intelligence and Lecture Notes in Bioinformatics)* (pp. 32-44).

Haindl, M., and Mikeš, S. (2016). A competition in unsupervised color image segmentation. *Pattern Recognition, 57*, 136-151. doi:10.1016/j.patcog.2016.03.003

Ho, F.-g., and Striender, W. (1981). A variational calculation of the effective surface diffusion coefficient and tortuosity. *Chemical Engineering Science, 36*(2), 253-258. doi:http://dx.doi.org/10.1016/0009-2509(81)85003-8

Hu, L. B., Savidge, C., Rizzo, D. M., Hayden, N., Hagadorn, J. W., & Dewoolkar, M. (2013). Commonly used porous building materials: Geomorphic pore structure and fluid transport. *Journal of Materials in Civil Engineering, 25*(12), 1803-1812. doi:10.1061/(ASCE)MT.1943-5533.0000706

Ilunga-Mbuyamba, E., Cruz-Duarte, J. M., Avina-Cervantes, J. G., Correa-Cely, C. R., Lindner, D., and Chalopin, C. (2016). Active contours driven by Cuckoo Search strategy for brain tumour images segmentation. *Expert Systems with Applications, 56*, 59-68. doi:10.1016/j.eswa.2016.02.048

Image Processing Toolbox User's Guide: bwmorph. Retrieved from http://matlab.izmiran.ru/help/toolbox/images/bwmorph.html

Iversen, N., and Jørgensen, B. B. (1993). Diffusion coefficients of sulfate and methane in marine sediments: Influence of porosity. *Geochimica et Cosmochimica Acta, 57*(3), 571-578. doi:http://dx.doi.org/10.1016/0016-7037(93)90368-7

J.C.Maxwell. (18763). A treatise on electricity and magnetism. *Clarendon Press,London, I*.

Joekar-Niasar, V., Doster, F., Armstrong, R. T., Wildenschild, D., and Celia, M. A. (2013). Trapping and hysteresis in two-phase flow in porous media: A pore-network study. *Water Resources Research, 49*(7), 4244-4256. doi:10.1002/wrcr.20313

Keller, L. M., Hilger, A., and Manke, I. (2015). Impact of sand content on solute diffusion in Opalinus Clay. *Applied Clay Science, 112-113*, 134-142. doi:10.1016/j.clay.2015.04.009

Koponen, A., Kataja, M., and Timonen, J. (1997). Permeability and effective porosity of porous media. *Physical Review E - Statistical Physics, Plasmas, Fluids, and Related Interdisciplinary Topics, 56*(3 B), 3319-3325.

Lanfrey, P. Y., Kuzeljevic, Z. V., and Dudukovic, M. P. (2010). Tortuosity model for fixed beds randomly packed with identical particles. *Chemical Engineering Science, 65*(5), 1891-1896. doi:10.1016/j.ces.2009.11.011

Larsbo, M., Koestel, J., and Jarvis, N. (2014). Relations between macropore network characteristics and the degree of preferential solute transport. *Hydrology and Earth System Sciences, 18*(12), 5255-5269. doi:10.5194/hess-18-5255-2014

Li, J. H., and Yu, B. M. (2011). Tortuosity of flow paths through a Sierpinski carpet. *Chinese Physics Letters, 28*(3). doi:10.1088/0256-307X/28/3/034701

Lindquist, W. B., Lee, S. M., Coker, D. A., Jones, K. W., and Spanne, P. (1996). Medial axis analysis of void structure in three-dimensional tomographic images of porous media. *Journal of Geophysical Research B: Solid Earth, 101*(4), 8297-8310.

Low, P. F. (1981). Principles of ion diffusion in clays. *In: Chemistry in the Soil Environment, American Society for Agronomy, Special Publication, 40*, 31-45.

Manickam, S. S., Gelb, J., and McCutcheon, J. R. (2014). Pore structure characterization of asymmetric membranes: Non-destructive characterization of porosity and tortuosity. *Journal of Membrane Science, 454*, 549-554. doi:10.1016/j.memsci.2013.11.044

Masciopinto, C., and Palmiotta, D. (2013). Flow and Transport in Fractured Aquifers: New Conceptual Models Based on Field Measurements. *Transport in Porous Media, 96*(1), 117-133. doi:10.1007/s11242-012-0077-y

Matyka, M., Khalili, A., & Koza, Z. (2008). Tortuosity-porosity relation in porous media flow. *Physical Review E - Statistical, Nonlinear, and Soft Matter Physics, 78*(2). doi:10.1103/PhysRevE.78.026306

Mauret, E., and Renaud, M. (1997). Transport phenomena in multi-particle systems—I. Limits of applicability of capillary model in high voidage beds-application to fixed beds of fibers and fluidized beds of spheres. *Chemical Engineering Science, 52*(11), 1807-1817. doi:http://dx.doi.org/10.1016/S0009-2509(96)00499-X

Maxwell, J. (1881). Treatise on Electricity and Magnetism. *second ed. Clarendon Press*.

Maxwell, J.C. 1873. A treatise on electricity and magnetism. Vol. I. Clarendon Press, London. (1873).

Millington, R. J. (1959). Gas diffusion in porous media. *Science, 130*(3367), 100-102.

Moldrup, P., Olesen, T., Komatsu, T., Schjønning, P., and Rolston, D. E. (2001). Tortuosity, diffusivity, and permeability in the soil liquid and gaseous phases. *Soil Science Society of America Journal, 65*(3), 613-623.

Morin, R. H., LeBlanc, D. R., and Troutman, B. M. (2010). The influence of topology on hydraulic conductivity in a sand-and-gravel aquifer. *Ground Water, 48*(2), 181-190. doi:10.1111/j.1745-6584.2009.00646.x

Morphological operations on binary images. (pp. 22-29).

Mota, Teixeira, J. A., and Yelshin, A. (2001). Binary spherical particle mixed beds porosity and permeability relationship measurement. . *Trans. Filtr. Soc., 1*, 1:101–106.

Naveed, M., Hamamoto, S., Kawamoto, K., Sakaki, T., Takahashi, M., Komatsu, T.,and De Jonge, L. W. (2013). Correlating gas transport parameters and x-ray computed tomography measurements in porous media. *Soil Science, 178*(2), 60-68. doi:10.1097/SS.0b013e318288784c

Neale, G. H., and Nader, W. K. (1973). Prediction of transport processes in porous media. *American Institute of Chemical Engineers Journal, 19*, 112–119.

Ngom, N. F., Garnier, P., Monga, O., and Peth, S. (2011). Extraction of three-dimensional soil pore space from microtomography images using a geometrical approach. *Geoderma, 163*(1–2), 127-134. doi:http://dx.doi.org/10.1016/j.geoderma.2011.04.013

Nimmo, J. R. (2004). Porosity and Pore Size Distribution *Encyclopedia of Soils in the Environment* (Vol. 3, pp. 295-303). London: Elsevier.

Nriagu, J. O. (1979). Geochemical processes, water and sediment environments: A. Lerman. Wiley, 1979, 481 pp. $29.95. *Geochimica et Cosmochimica Acta, 43*(11), 1869-1870. doi:http://dx.doi.org/10.1016/0016-7037(79)90038-3

Oliveira, R. B., Filho, M. E., Ma, Z., Papa, J. P., Pereira, A. S., and Tavares, J. M. R. S. (2016). Computational methods for the image segmentation of pigmented skin lesions: A review. *Computer Methods and Programs in Biomedicine, 131*, 127-141. doi:10.1016/j.cmpb.2016.03.032

Pardo-Alonso, S., Vicente, J., Solórzano, E., Rodriguez-Perez, M. Á., and Lehmhus, D. (2014). Geometrical Tortuosity 3D Calculations in Infiltrated Aluminium Cellular Materials. *Procedia Materials Science, 4,* 145-150. doi:http://dx.doi.org/10.1016/j.mspro.2014.07.553

Pech. (1984). *Etude de la permiabilité des lits compressibles constitués de copeaux de bois partiellement destructurés*. Retrieved from Grenoble, France:

Peng, S., Marone, F., and Dultz, S. (2014). Resolution effect in X-ray microcomputed tomography imaging and small pore's contribution to permeability for a Berea sandstone. *Journal of Hydrology, 510*, 403-411. doi:10.1016/j.jhydrol.2013.12.028

Petersen, L. W., Moldrup, P., Jacobsen, O. H., and Rolston, D. E. (1996). Relations between specific surface area and soil physical and chemical properties. *Soil Science, 161*(1), 9-20.

Pisani, L. (2011). Simple Expression for the Tortuosity of Porous Media. *Transport in Porous Media, 88*(2), 193-203. doi:10.1007/s11242-011-9734-9

Prodanovic, M., and Lindquist, B. 3DMA-Rock Primer. Retrieved from http://www.ams.sunysb.edu/~lindquis/3dma/3dma_rock/3dma_rock_03_primer/primer.html

Promentilla, M. A. B., Sugiyama, T., Hitomi, T., and Takeda, N. (2009). Quantification of tortuosity in hardened cement pastes using synchrotron-based X-ray computed microtomography. *Cement and Concrete Research, 39*(6), 548-557. doi:10.1016/j.cemconres.2009.03.005

Rayleigh, L. (1892). On the influence of obstacles arranged in rectangular order upon the properties of a medium. *Philosophical Magazine, 34*, 481–489.

Reed, A. H., Thompson, K. E., Briggs, K. B., and Willson, C. S. (2010). Physical pore properties and grain interactions of SAX04 sands. *IEEE Journal of Oceanic Engineering, 35*(3), 488-501. doi:10.1109/JOE.2010.2040656

Rezaee, M. R., Motiei, H., and Kazemzadeh, E. (2007). A new method to acquire m exponent and tortuosity factor for microscopically heterogeneous carbonates. *Journal of Petroleum Science and Engineering, 56*(4), 241-251. doi:10.1016/j.petrol.2006.09.004

Saha, P. K., Borgefors, G., and Sanniti di Baja, G. (2015). A survey on skeletonization algorithms and their applications. *Pattern Recognition Letters*. doi:10.1016/j.patrec.2015.04.006

Salmas, C., and Androutsopoulos, G. (2001). Mercury porosimetry: Contact angle hysteresis of materials with controlled pore structure. *Journal of Colloid and Interface Science, 239*(1), 178-189. doi:10.1006/jcis.2001.7531

Salmas, C. E., and Androutsopoulos, G. P. (2001). A novel pore structure tortuosity concept based on nitrogen sorption hysteresis data. *Industrial and Engineering Chemistry Research, 40*(2), 721-730.

Shanti, N. O. (2010). *Microstructurally tailored ceramics for advanced energy applications by thermoreversible gelcasting.* Northwestern University.

Shanti, N. O., Chan, V. W. L., Stock, S. R., De Carlo, F., Thornton, K., and Faber, K. T. (2014). X-ray micro-computed tomography and tortuosity calculations of percolating pore networks. *Acta Materialia, 71*, 126-135. doi:10.1016/j.actamat.2014.03.003

Shen, L., and Chen, Z. (2007). Critical review of the impact of tortuosity on diffusion. *Chemical Engineering Science, 62*(14), 3748-3755. doi:10.1016/j.ces.2007.03.041

Soukup, K., Hejtmánek, V., Čapek, P., Stanczyk, K., and Šolcová, O. (2015). Modeling of contaminant migration through porous media after underground coal gasification in shallow coal seam. *Fuel Processing Technology, 140*, 188-197. doi:10.1016/j.fuproc.2015.08.033

Su, L. J., Zhang, Y. J., and Wang, T. X. (2014). Investigation on permeability of sands with different particle sizes. *Yantu Lixue/Rock and Soil Mechanics, 35*(5), 1289-1294.

Sun, Z., Tang, X., and Cheng, G. (2013). Numerical simulation for tortuosity of porous media. *Microporous and Mesoporous Materials, 173*, 37-42. doi:http://dx.doi.org/10.1016/j.micromeso.2013.01.035

Takahashi, H., Seida, Y., and Yui , M. (2009). 3D X-ray CT and diffusion measurements to assess tortuosity and constrictivity in a sedimentary rock. *The Open-Access Journal for the Basic Principles of Diffusion Theory, Experiment and Application, 11*(89), 1-11.

Theng, B. K. G., Ristori, G. G., Santi, C. A., and Percival, H. J. (1999). An improved method for determining the specific surface areas of topsoils with varied organic matter content, texture and clay mineral composition. *European Journal of Soil Science, 50*(2), 309-316. doi:10.1046/j.1365-2389.1999.00230.x

Thorp, K. R., Wang, G., Badaruddin, M., and Bronson, K. F. (2016). Lesquerella seed yield estimation using color image segmentation to track flowering dynamics in response to variable water and nitrogen management. *Industrial Crops and Products, 86*, 186-195. doi:10.1016/j.indcrop.2016.03.035

Touil, A., and Kalti, K. (2016). Iterative fuzzy segmentation for an accurate delimitation of the breast region. *Computer Methods and Programs in Biomedicine, 132*, 137-147. doi:10.1016/j.cmpb.2016.04.020

Ullman, W. J., and Aller, R. C. (1982). Diffusion coefficients in near shore marine sediments. *Limnology Oceanography, 27*, 552-556.

van Brakel, J., and Heertjes, P. M. (1974). Analysis of diffusion in macroporous media in terms of a porosity, a tortuosity and a constrictivity factor. *International Journal of Heat and Mass Transfer, 17*(9), 1093-1103. doi:10.1016/0017-9310(74)90190-2

Vepraskas, M. J., and Cassel, D. K. (1987). Sphericity and roundness of sand in coastal plain soils and relationships with soil physical properties. *Soil Science Society of America Journal, 51*(5), 1108-1112.

Vervoort, R. W., and Cattle, S. R. (2003). Linking hydraulic conductivity and tortuosity parameters to pore space geometry and pore-size distribution. *Journal of Hydrology, 272*(1-4), 36-49. doi:10.1016/S0022-1694(02)00253-6

Villa-Vélez, H. A., Váquiro, H. A., Bon, J., and Telis-Romero, J. (2012). Modelling thermodynamic properties of banana waste by analytical derivation of desorption isotherms. *International Journal of Food Engineering, 8*(1). doi:10.1515/1556-3758.2191

Watanabe, Y., and Nakashima, Y. (2002). RW3D.m: three-dimensional random walk program for the calculation of the diffusivities in porous media. *Computers & Geosciences, 28*(4), 583-586. doi:http://dx.doi.org/10.1016/S0098-3004(01)00057-7

Weissberg, H. (1963). Effective diffusion coefficients in porous media. *Journal of Applied Physics*, *34*, 2636–2639.

Wong, H. Y. (2016). Parameters affecting compaction in Hong Kong soils. *HKIE Transactions Hong Kong Institution of Engineers, 23*(3), 157-170. doi:10.1080/1023697X.2016.1204702

Yongjin, F., and Boming, Y. (2007). Fractal dimension for tortuous streamtubes in porous media. *Fractals*, *15*(4), 385-390.

Yu, B. M., and Li, J. H. (2004). A geometry model for tortuosity of flow path in porous media. *Chinese Physics Letters, 21*(8), 1569-1571. doi:10.1088/0256-307X/21/8/044

Yuan, Y., Gholizadeh Doonechaly, N., and Rahman, S. (2016). An Analytical Model of Apparent Gas Permeability for Tight Porous Media. *Transport in Porous Media, 111*(1), 193-214. doi:10.1007/s11242-015-0589-3

Yukselen-Aksoy, Y., and Kaya, A. (2010). Predicting soil swelling behaviour from specific surface area. *Proceedings of the Institution of Civil Engineers: Geotechnical Engineering, 163*(4), 229-238. doi:10.1680/geng.2010.163.4.229

Appendix A: Image Processing and Geometrical Parameters Calculations

Segmentation was performed on raw micro-tomography images that were scaled to intensity value of 0-255 to separate the void and solid phases. Segmentation process was implemented through the following steps (Al-Raoush, 2014):

- **First step**: images scanned at 33.069 keV energy were used to identify solid phase.
- **Second Step**: Indicator Kriging Algorithm (IKA) was implemented to identify the two phases, the pore and solid phases [94].
- **Third step**: The IKA separated the phases based on intensity values I_1 and I_2 obtained from histogram of intensity. Voxels that had intensity greater than I_1 were assigned to one phase and intensity less than voxels that had I_2 were assigned to second phase. Voxels between I_1 and I_2 were assigned to wither phase based on the maximum likehood estimate of each phase obtained from the two-point correlation function [94].
- **Fourth step**: Watershed –transform was applied to identify sand grains [94].

Determination of Geometrical Parameters

Porosity was computed as the ratio of the voxels of the void space of the total voxels of the image.

The diameter of a grain computed was a follows:

$$D = 2.\left(\prod_{BV=1}^{N^{BV}} d^{C,BV}\right)^{1/N^{BV}}$$

Where $d^{C,BV}$ is the Euclidean distance between the center of the grain, C, and a boundary voxel of the grain, BV, and N^{BV} is the total number of boundary voxels of the grain. A boundary voxel connects the grain to other phases through a face, an edge or a corner and was determined by an algorithm that searched its twentysix neighbouring voxels. The center of the grain computed was as follows:

$$C_i = \frac{\sum_i i}{V_p}, for\ i = x, y, z$$

Where x, y and z are now, column and depth indices, and C_p is the volume of the grain computed as its total number of voxels. The distance, $d^{C,BV}$, was computed using the Euclidean metric as follows:

$$d^{C,BV} = \left((C_x - BV_x)^2 + \left(C_y - BV_y\right)^2 + (C_z - BV_z)^2\right)^{1/2}$$

Appendix B: Image Processing Steps

REV Plot

```
> load col43R_seg_3D

>> image_rev=seg_volume(331:350,371:387,195:220);

>>
v=length(find(image_rev(:,:,:)==0))+length(find(image_rev(:,:,:)==3))+length(find(image_rev(:,:,:)
==1))

>> all=length(image_rev(:))

all =

>> v/all

load col43R_seg_3D

imagesc( seg_volume (:,:,1))

whos

image_rev=seg_volume(141:540,179:523,:);

% image_rev=seg_volume(151:530,191:518,14:507);

% image_rev=seg_volume(161:520,201:511,25:492);

% image_rev=seg_volume(171:510,211:503,35:476);

% image_rev=seg_volume(181:500,221:496,45:460);

% image_rev=seg_volume(191:490,231:489,55:444);

% image_rev=seg_volume(201:480,241:482,65:428);

% image_rev=seg_volume(211:470,251:474,75:412);

% image_rev=seg_volume(221:460,261:467,85:396);

% image_rev=seg_volume(231:450,271:460,95:380);

%image_rev=seg_volume(241:440,281:453,105:364);
```

```
% image_rev=seg_volume(251:430,291:445,115:348);

% image_rev=seg_volume(261:420,301:438,125:332);

%image_rev=seg_volume(271:410,311:431,135:316);

% image_rev=seg_volume(281:400,321:424,145:300);

% image_rev=seg_volume(291:390,331:416,155:284);

% image_rev=seg_volume(301:380,341:409,165:268);

% image_rev=seg_volume(311:370,351:402,175:252);

% image_rev=seg_volume(321:360,361:395,185:236);

% image_rev=seg_volume(331:350,371:387,195:220);

%imagesc( image_rev(:,:,1))

whos
```

Models Generated - Void

```
x=[0.3311 0.4334 1.8584 1.1462 0.9142 0.8353 212.788224 1.56E+01; 0.371 0.3518 1.8472 1.1178 0.9027 0.8272 248.32512 1.95E+01; 0.3295 0.2705 1.7926 1.0586 0.8896 0.8148 316.412928 2.35E+01; 0.3536 0.2672 1.7938 1.0682 0.8877 0.812 340.34688 2.62E+01; 0.3189 0.2581 1.8312 1.0042 0.8902 0.8152 315.076608 2.27E+01; 0.3793 0.1957 1.5242 1.0863 0.8825 0.8068 450.680832 3.60E+01; 0.4557 0.2756 2.4936 1.0618 0.8154 0.725 276.84864 2.55E+01; 00.4901 0.2371 1.9531 1.074 0.8181 0.7143 335.609856 3.25E+01; 0.4933 0.1785 1.7204 1.0591 0.8131 0.7269 406.573056 4.09E+01; 0.3976 0.2982 2.4607 1.0641 0.8416 0.757 274.305024 2.28E+01; 0.4029 0.2524 1.9586 1.0936 0.8517 0.7721 341.001216 2.87E+01; 0.3893 0.2304 1.8912 1.0303 0.8559 0.7742 345.074688 2.85E+01; 0.43 0.185 1.5895 1.0575 0.8505 0.7709 434.912256 3.93E+01];

y=[ 1.5639; 1.4626; 1.4173; 1.426; 1.505; 1.4086; 1.5704; 1.6327; 1.5666; 1.5691; 1.5644; 1.5775; 1.533];

>> modelfun = @(b,x) (( b(1)*x1.^b(2)).*(x2.^b(3)).*(x3.^b(4)).*(x4.^b(5)).*(x5.^b(6)).*(x6.^b(7)).*(x8.^b(8))+b(9));

>> modelfun = @(b,x) (b(1)*x1.^b(2)+x1.^2 +b(3));
```

```
b=[1;1;1];

x1= x(:,1);

x2= x(:,2);

x3= x(:,3);

x4= x(:,4);

x5= x(:,5);

x6= x(:,6);

x8= x(:,8);

beta0 =[1;1;1];

beta = nlinfit(x,y,modelfun,beta0)

 [ahat,r,J,cov,mse] = nlinfit(x,y,modelfun,beta0);

>> ahat

>>  ci = nlparci(ahat,r,'Jacobian',J)

yr=modelfun(beta,x);

Rsq1 = 1 - sum((y-yr).^2)/sum((y-mean(y)).^2)


plot(yr,y,'o')

>> xs=[1   1.6  1.8];

>> ys=xs;

>> hold on

>> plot(xs,ys)

>> residual=y-yr;

>> plot(yr,residual,'o')

>> xa=[1.4  1.8];
```

```
>> ya=[0  0];

>> hold on

>> plot(xa,ya)

z=normplot(residual)
```

Calculating Residual %

```
seg_volume_system_for_analysis=seg_volume(151:530,191:570,:);

void=length(find(seg_volume_system_for_analysis(:,:,:)==0))+length(find(seg_volume_system_for_analysis (:,:,:)==3))+length(find(seg_volume_system_for_analysis (:,:,:)==1))

void_without_fluid_or_water=length(find(seg_volume_system_for_analysis(:,:,:)==0))

void_without_fluid_or_water_to_void= void_without_fluid_or_water/void

fluid= length(find(seg_volume_system_for_analysis (:,:,:)==3))

fluid_to_void=fluid/void

water= length(find(seg_volume_system_for_analysis (:,:,:)==1))

water_to_void=water/void

water_to_fluid_percentage=100*water/fluid
```

Images for Studying the Impact of Trapped Oil on Tortuosity

```
>> seg_volume_new_pixel=seg_volume;

% Change the pixel value of water to the pixel value of void

>> seg_volume_new_pixel( seg_volume_new_pixel(:,:,:)==1)=0;

%Change the pixel value of fluid to pixel value of solid

>> seg_volume_new_pixel( seg_volume_new_pixel(:,:,:)==3)=2;

% Change pixel value of solid from 2 to 1

>> seg_volume_new_pixel( seg_volume_new_pixel(:,:,:)==2)=1;

save seg_volume_new_pixel seg_volume_new_pixel
```

```
imagesc( seg_volume_new_pixel(:,:,1))

>> impixelinfo

% Change the size of the image to 380x380x520

>> raw_image=seg_volume_new_pixel(151:530,191:570,:);

>> save raw_image raw_image

imagesc(raw_image(:,:,1))
```

Appendix C: Random Paths Code

```
    % Initial Setup


    nrows=size(raw_image,1);
    ncolumns=size(raw_image,2);
    ndepth=size(raw_image,3);


  %  N=(2)^3;

    void_list_index=find(raw_image(:,:,1)==0);

    %initial_pointer=ranomperm(length(void_list_index));

  % initial_pointer= void_list_index(randi(size(void_list_index,1)),:);

  %  for particle_id=1:100;

      %
initial_position_index=void_list_index(initial_pointer(particle_id));

   % end

     initial_position_index=void_list_index(47134);

      next_move=[];

    depth=1;

    z_initial_position_index=floor(((initial_position_index)-
1)/(nrows*ncolumns))+1;
    y_initial_position_index=ceil(initial_position_index/nrows)-
(ncolumns*(z_initial_position_index-1));
    x_initial_position_index=(initial_position_index-
nrows*(y_initial_position_index-1)-
nrows*ncolumns*(z_initial_position_index-1));

   initial_position_location=[x_initial_position_index
y_initial_position_index  z_initial_position_index];

  %  for Particle_ID=1:1
          % length(initial_position_index);

  connect=26;
```

```
 while depth <=750
      %    while depth ~=15 % depth should be ndepth = 300


    [neighbor_voxels]=get_connect_index_torto(nrows,ncolumns,ndepth,
initial_position_location(end,:),connect);

    initial_position_location_index=
initial_position_location(:,1)+nrows*(initial_position_location(:,2)-
1)+nrows*ncolumns*(initial_position_location(:,3)-1);


neighbor_voxels(find(neighbor_voxels==initial_position_location_index(e
nd)))=[];


    neighbor_voxels_check=raw_image(neighbor_voxels);

    neighbor_voxels_void_pointer=find(neighbor_voxels_check ==0);


neighbor_voxels_void_index=neighbor_voxels(neighbor_voxels_void_pointer
);

   z_neighbor_voxels=floor(((neighbor_voxels_void_index)-
1)/(nrows*ncolumns))+1;
   y_neighbor_voxels=ceil(neighbor_voxels_void_index/nrows)-
(ncolumns*(z_neighbor_voxels-1));
   x_neighbor_voxels=neighbor_voxels_void_index-
nrows*(y_neighbor_voxels-1)-nrows*ncolumns*(z_neighbor_voxels-1);

   neighbor_voxels_location=[x_neighbor_voxels  y_neighbor_voxels
z_neighbor_voxels];

   if length(neighbor_voxels_void_pointer)>=1

    voxels_location_max_z_neighbor_voxels=
neighbor_voxels_location(z_neighbor_voxels==max(z_neighbor_voxels),:);

     %voxels_location_max_z_neighbor_voxels=
neighbor_voxels_location(randi(size(neighbor_voxels_location,1)),:);

   temp_next_move_location =
voxels_location_max_z_neighbor_voxels(randi(size(voxels_location_max_z_
neighbor_voxels,1)),:);

   next_move= [next_move ;temp_next_move_location];

   z_next_move=next_move(:,3);
```

```
   y_next_move=next_move(:,2);

   x_next_move=next_move(:,1);


   next_move_location = [x_next_move  y_next_move   z_next_move];


   else

        neighbor_voxels_soild_pointer= find( neighbor_voxels_check
==1);

       if length(neighbor_voxels_void_pointer(end,:))<1
           %find( neighbor_voxels_check ==1)==0
           %
          temp_next_move_location=temp_next_move_location(end-1,:);
          next_move=next_move(end-1,:);
          m=7;

       % temp_next_move_location =
neighbor_voxels_location(randi(find(neighbor_voxels_location==0)));

       % next_move= [next_move ;temp_next_move_location];
       end

   end
   %  initial_position_location=next_move_location;
       depth=depth+1;

 end


    distance= (sum((x_next_move(2:end)-x_next_move(1:end-1) ).^2) +
sum((y_next_move(2:end)-y_next_move(1:end-1) ).^2)
+sum((z_next_move(2:end)-z_next_move(1:end-1) ).^2));

    %distance= (sum((x_next_move(2:end)-x_next_move(1:end-1)
).^2)+(x_next_move(1)-x_initial_position_index)^2 +
sum((y_next_move(2:end)-y_next_move(1:end-1) ).^2) +(y_next_move(1)-
y_initial_position_index)^2 +sum((z_next_move(2:end)-z_next_move(1:end-
1) ).^2))+(z_next_move(1)-z_initial_position_index)^2;


    tortuosity_z= sqrt(distance)/(300-1);


    initial_position_location_1 = [ 1  1  12];
```

```
    [neighbor_voxels_1]=get_connect_index_torto(nrows,ncolumns,ndepth,
initial_position_location_1,connect);


    neighbor_voxels_check_1=raw_image(neighbor_voxels_1);

    neighbor_voxels_void_pointer_1=find(neighbor_voxels_check_1 ==0);


neighbor_voxels_void_index_1=neighbor_voxels_1(neighbor_voxels_void_poi
nter_1);

     z_neighbor_voxels_1=floor(((neighbor_voxels_void_index_1)-
1)/(nrows*ncolumns))+1;
   y_neighbor_voxels_1=ceil(neighbor_voxels_void_index_1/nrows)-
(ncolumns*(z_neighbor_voxels_1-1));
   x_neighbor_voxels_1=neighbor_voxels_void_index_1-
nrows*(y_neighbor_voxels_1-1)-nrows*ncolumns*(z_neighbor_voxels_1-1);

   neighbor_voxels_location_1=[x_neighbor_voxels_1  y_neighbor_voxels_1
z_neighbor_voxels_1];
```